

How Does the Eye Warm? Part II: Sensitivity to Vertical Wind Shear and a Trajectory Analysis

DANIEL P. STERN AND FUQING ZHANG

Department of Meteorology, The Pennsylvania State University, University Park, Pennsylvania

(Manuscript received 21 September 2012, in final form 1 January 2013)

ABSTRACT

In Part II of this study, idealized simulations of tropical cyclones are used to investigate the influence of vertical wind shear on the structure of warming and descent in the eye; results are compared with the no-shear simulation that was analyzed in Part I. During intensification of a tropical cyclone in a quiescent environment, time-averaged eye descent is maximized at 12–13-km height. Warming is not generally maximized at these levels, however, because the static stability is at a minimum. Consequently, the perturbation temperature is maximized at midlevels. Each of the above results remains valid for sheared tropical cyclones, and therefore shear does not systematically alter the height of the warm core.

An analysis of over 90 000 parcel trajectories yields further insight into the mechanisms of eye warming and addresses several outstanding questions regarding the character of eye descent. The rate at which parcels are stirred from the eye into the eyewall is a strong function of intensity. While stirring is large at the beginning of rapid intensification (RI), once a sufficient intensity is achieved, most parcels originating near the storm center can remain inside the eye for at least several days. Many parcels in the upper troposphere are able to descend within the eye by 5–10 km. The above results are relatively insensitive to the presence of up to 10 m s⁻¹ of shear. In contrast, stirring in the eye–eyewall interface region is substantially enhanced by shear.

1. Introduction

This is the second part of a two-part investigation into the dynamics and structure of the eye of tropical cyclones (TCs). In Stern and Zhang (2013, hereafter Part I), we investigated the mechanisms by which the tropical cyclone eye warms, through a potential temperature (θ) budget analysis of an idealized tropical cyclone simulated in a quiescent environment. As further summarized below, we showed that the perturbation temperature is warmest at midlevels because the advection of θ is strongest in this region during the period of most rapid intensification. Additionally, we found that the relative contribution of various terms to the budget (in particular, subgrid-scale horizontal diffusion) varies greatly with intensity. In this Part II, we further examine the structure and dynamics of the eye through trajectory analyses, and we extend our previous analyses to include simulations of hurricanes within environments containing vertical wind shear.

Stern and Nolan (2012, hereafter SN12) showed that the perturbation temperature (i.e., the “warm core”) in simulated tropical cyclones tends to be warmest at midlevels (4–8 km), contrary to what is widely believed to be a preferred upper-level maximum (e.g., Halverson et al. 2006; Holland 1997; Knaff et al. 2004). In Part I, we showed that this midlevel maximum in perturbation temperature is a consequence of the fact that the rate of warming of the eye during the period of rapid intensification (RI) is itself maximized at midlevels. A potential temperature budget analysis was performed on a simulation of a TC in a quiescent environment, and it was found that although mean vertical advection was indeed responsible for the bulk of eye warming during the latter part of RI, there was a 12–18-h period during the beginning of RI where warming was due mainly to the convergence of the radial eddy flux of θ , likely related to a wavenumber-1 instability (Nolan et al. 2001). An important result is that net warming can and occasionally does occur where there is mean ascent in the eye.

In Part I, it was shown that mean vertical advection of potential temperature (and mean descent itself) becomes concentrated along the eye–eyewall interface once a

Corresponding author address: Dr. Daniel P. Stern, Department of Meteorology, The Pennsylvania State University, University Park, PA 16802.
E-mail: dps19@psu.edu

sufficient intensity is reached.¹ The resulting temperature tendencies remain very large in this region even during periods of quasi-steady state or weakening intensity. The reason this interface region does not continue to warm (and for most heights is not at any time the radial location of maximum warming) is that the warming tendency from descent is nearly entirely offset by the cooling tendency from evaporatively driven diabatic cooling, mean radial advection, and parameterized horizontal diffusion. In particular, once the intensity of the simulated storm exceeds about 50 m s^{-1} , horizontal diffusion becomes a leading order term in the budget of potential temperature in a region extending well into the interior of the eye.

In this Part II, we investigate the structure of warming and descent in the eye of idealized tropical cyclones that are embedded within vertically sheared environmental flows. To gain further insight into the dynamics of the eye, we then examine an extensive set of parcel trajectories for air within the eye for both the original and the new simulations. A brief overview of the model setup and a description of the new simulations, as well as an analysis of the structure of warming and mean descent for these simulations, is given in section 2. Also in section 2, we examine the θ budget for a sheared simulation and compare to that of the no-shear simulation that was analyzed in Part I. We present the results of our trajectory analyses in section 3. A discussion and conclusions are given in section 4.

2. Structure and evolution of simulations with shear

a. Model setup and description of simulations

As in Part I, we use the Weather Research and Forecasting model (WRF), v3.1.1, to simulate the evolution of an idealized tropical cyclone on a doubly periodic f plane ($f = 5.0 \times 10^{-5} \text{ s}^{-1}$), in a thermodynamic environment given by the moist tropical sounding of Dunion (2011), and with SST = 28°C . In Part I, a single simulation in a quiescent environment was examined (NOFLOW). Here, we also examine two additional simulations. These new simulations have 5 m s^{-1} easterly flow below 850 mb, and either 5 m s^{-1} (SHEAR5) or 10 m s^{-1} (SHEAR10) of westerly shear between 850 and 200 mb (with winds varying linearly in log pressure, and thus approximately

¹ Generally, there are two mechanisms that have been proposed for driving this concentrated descent: as a balanced response to eyewall heating for certain distributions of inertial stability (Schubert et al. 2007), and as the local result of negative buoyancy from evaporative cooling (Liu et al. 1999). Further discussion of these mechanisms can be found in Part I and in Willoughby (1998).

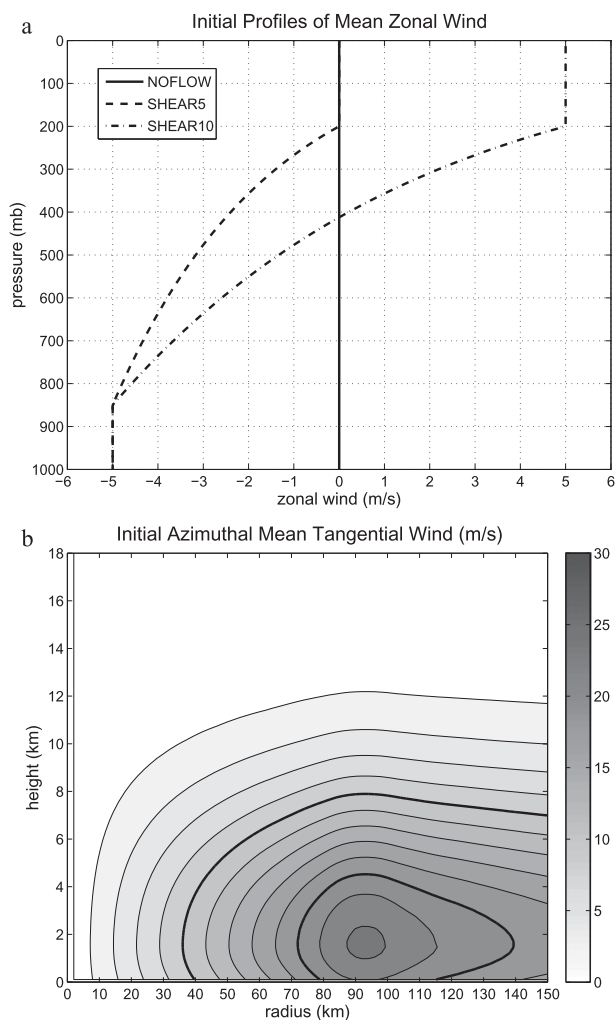


FIG. 1. (a) The initial vertical profiles of the mean zonal winds (m s^{-1}) in each simulation, and (b) the initial radius–height structure of the azimuthal-mean tangential winds (identical in all simulations). In (b), the contour interval is 2 m s^{-1} , and the 10 and 20 m s^{-1} contours are thickened.

linearly in height). The environmental flow is constant with height above 200 mb. All other aspects of the setup of these simulations are identical to those of NOFLOW and are given in Part I.

Figure 1 shows vertical profiles of the initial zonal component of the environmental winds for each of the simulations (the meridional component is zero), as well as the initial radius–height structure of the azimuthal-mean tangential wind (identical in each simulation). The simulations are initialized using the method of “point downscaling” (Nolan 2011), whereby a single profile of temperature, humidity, and wind is used to define a horizontally homogeneous environment into which a balanced vortex is embedded. For environments with nonzero winds and vertical wind shear, this would generally

require there to be environmental pressure and temperature gradients, respectively, and these are incompatible with periodic boundary conditions. In point downscaling, the environment is kept homogeneous, and a fictitious pressure force is added to the meridional momentum equation (for zonal winds/shear) to balance the background wind field in the absence of real pressure and temperature gradients (Nolan and Rappin 2008; Rappin et al. 2010). While the neglect of environmental temperature gradients does affect the favorability for intensification, Nolan (2011) showed that for values of shear that were not so strong so as to completely prevent intensification, the structure and evolution of vortices was similar when using point downscaling versus using “real shear.”

b. Evolution of intensity

The time series of intensity in terms of maximum 10-m wind speed $V_{\max 10}$ and minimum sea level pressure P_{\min} for each of these three simulations is shown in Fig. 2, along with the track of the surface center (defined by the minimum of the surface pressure field, after being horizontally smoothed 500 times with a 1:2:1 smoother). Somewhat surprisingly, all simulations achieve approximately the same quasi-steady intensity ($\sim 70 \text{ m s}^{-1}$) after about 5 days, in spite of the vertical wind shear that is present in SHEAR5 and SHEAR10. Observationally, it is well known that shear is an important inhibiting factor for intensity (Black et al. 2002; Kaplan and DeMaria 2003; Kaplan et al. 2010). On the other hand, it is also understood from a theoretical perspective that strong hurricanes are intrinsically resilient to shear (Reasor et al. 2004). Further, Zeng et al. (2007) showed (for storms in the western North Pacific) that while on average, intensity decreases with increasing shear, the maximum observed intensity is nearly constant up to about 20 m s^{-1} of shear.

In the context of previous numerical simulations, results regarding the sensitivity of intensity to shear are mixed. Frank and Ritchie (2001) found that even small values of vertical wind shear (5 m s^{-1}) eventually led to a rapid weakening of their simulated hurricane, and Kimball and Evans (2002) found that 2.5 m s^{-1} of shear resulted in a quasi-steady intensity that was about 35 mb weaker than for a simulation without shear. In the simulations of Wong and Chan (2004) on the other hand, shear of up to 4 m s^{-1} only led to a transient weakening and did not change the quasi-steady intensity achieved. Recently, Riemer et al. (2010) presented a set of simulations where even 15 m s^{-1} of shear yielded a quasi-steady intensity only 5 m s^{-1} weaker than without shear. While it is not the purpose of this paper to investigate the relationship between intensity and shear, the above

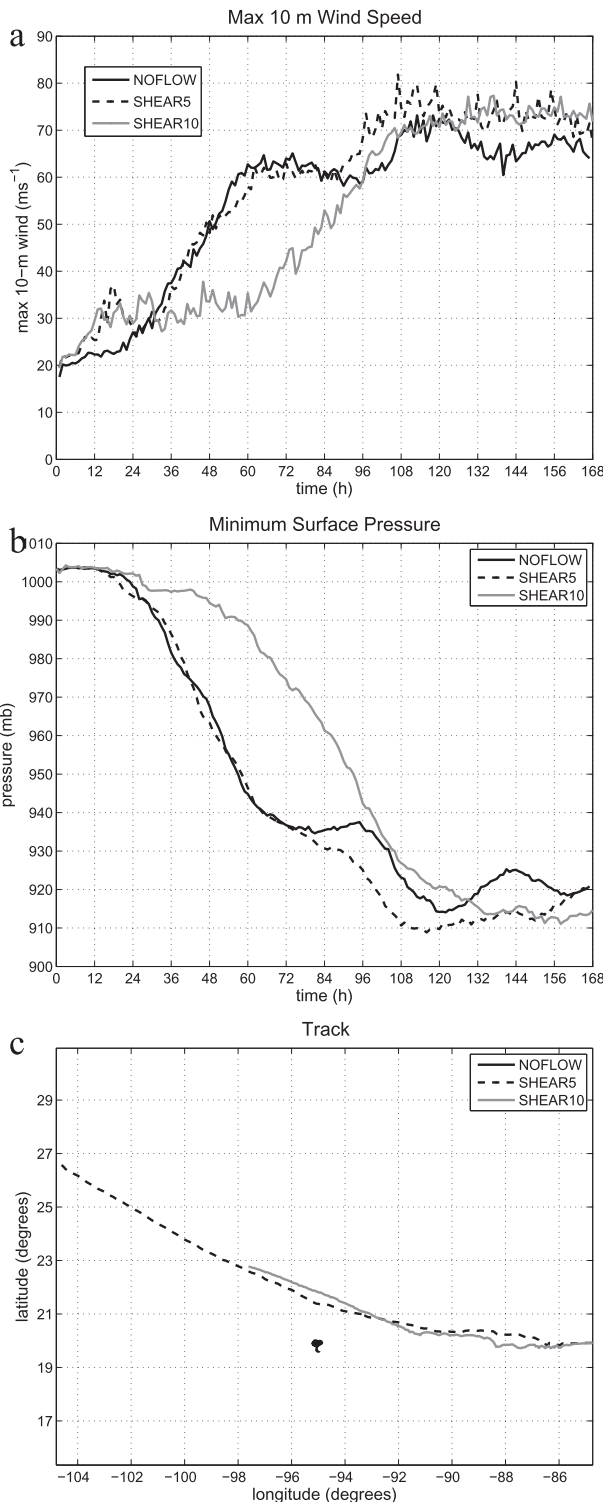


FIG. 2. For each of the simulations, time series of (a) maximum 10-m wind speed and (b) minimum sea level pressure, and (c) the track of the storm center (see text for definition). Note that NOFLOW is initialized in the center of the outer domain, whereas SHEAR5 and SHEAR10 are initialized near the eastern edge of the outer domain.

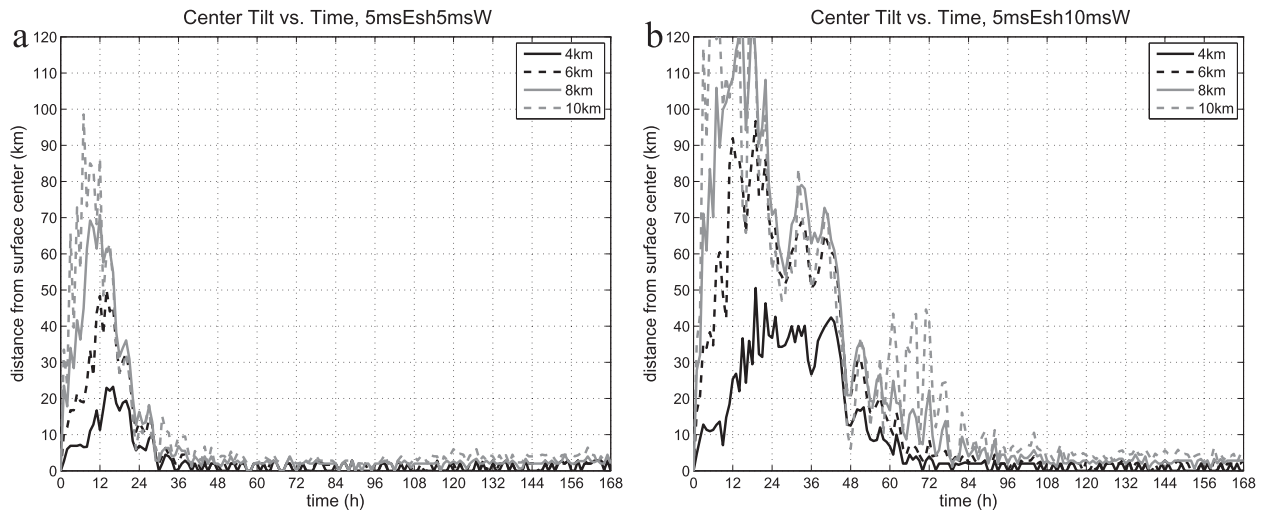


FIG. 3. Time series of the displacement of the center at varying heights from the surface center for (a) SHEAR5 and (b) SHEAR10.

review indicates that the intensity evolution of our sheared simulations is reasonable, given current knowledge.²

Although the quasi-steady intensities are similar, there is a 36-h delay in the onset of rapid intensification (RI) in SHEAR10 as compared to the other simulations. Further evidence of the effect of shear can be seen by comparing the time series of the magnitude of the tilt of the centers³ with height between SHEAR5 and SHEAR10 (Fig. 3). In SHEAR5, the tilt peaks at 12–15 h, and then decreases rapidly by 24 h, and the tilt between the surface and 10-km centers is quasi steady at about 5 km thereafter. The time when the tilt becomes small coincides with the start of RI. In contrast, in SHEAR10, the tilt remains relatively large until 48–60 h, and RI does not begin until about 60 h. In both cases, the midlevel center precesses cyclonically from downshear to left of shear (relative to the surface center), and the time at which the tilt vector achieves a left-of-shear orientation corresponds to the beginning of the rapid reduction of tilt, and slightly precedes the onset of RI (not shown). This relationship between precession, tilt, and the onset of RI is consistent with

² We believe that the balance of evidence from the more recent studies suggests that for moderate values, shear itself does not substantially reduce the maximum achievable intensity of tropical cyclones. The reason that shear does indeed lead to a reduced intensity most of the time is likely due to the ability to advect dry air into the core of the TC (e.g., Tang and Emanuel 2012). While regions of very dry air are quite common in the environments of TCs, they are absent in these idealized simulations.

³ Above the surface, the center is defined as the minimum in the smoothed geopotential height field valid on constant pressure surfaces corresponding to the mean pressure of each model level. These centers are then interpolated to a regular array of heights.

what has been shown recently in Rappin and Nolan (2012) and Zhang and Tao (2013).

c. Structure of temperature and vertical velocity in the eye

In Part I, we showed that in NOFLOW, the perturbation temperature was always greatest at midlevels (4–8-km height), and that this was consistent with the results of SN12, who found that such a structure was generally seen across a large number of idealized simulations. Figure 4 shows time–height Hovmöller plots of the perturbation temperature at the (surface) center of NOFLOW and each of the sheared simulations. It is clear that the sheared simulations are consistent with the results of SN12 and Part I, in that the perturbation temperature is maximized at midlevels. Therefore, it appears that shear itself does not have any obvious systematic effect on the height of the warm core.

Figure 5 shows the changes in azimuthal-mean potential temperature $\Delta\theta$ for the three 12-h periods of greatest intensity change for each of the simulations (0000 UTC day 2–1200 UTC day 3 for NOFLOW and SHEAR5; 1200 UTC day 3–0000 UTC day 5 for SHEAR10). The height at which $\Delta\theta$ is a maximum varies with time and among the simulations. Yet the overall pattern remains similar: there tends to be two distinct maxima in warming, one in midlevels (4–8 km) and another in upper levels (12–15 km), and the midlevel maximum is more often greater in magnitude. This leads to the preference for a midlevel maximum in perturbation temperature in each simulation.

The distribution of descent in the eye has a substantial influence on the distribution of warming. In Part I, we found that during the periods of RI, azimuthal-mean descent in the eye was strongest near 12–13-km height.

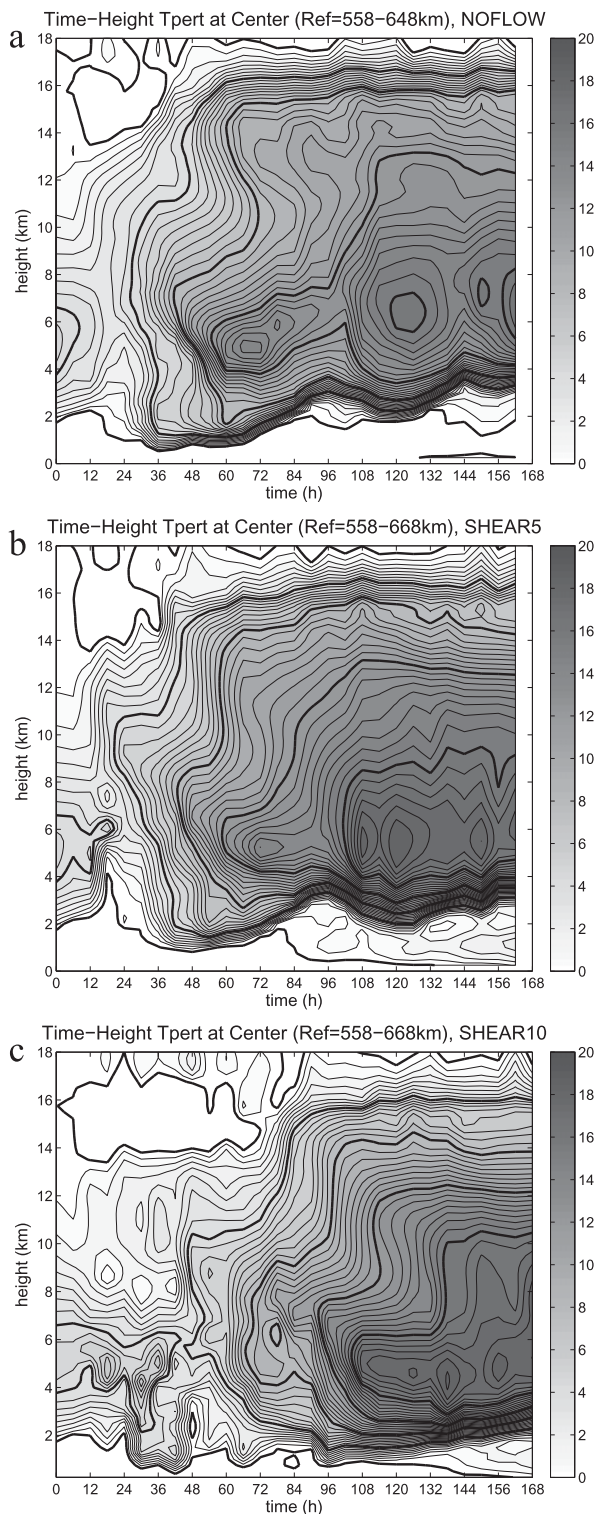


FIG. 4. Time–height Hovmöller plots of the perturbation temperature at the storm center for (a) NOFLOW, (b) SHEAR5, and (c) SHEAR10. The contour interval is 0.5°C, and every 4.0°C is contoured in thick black, starting at 0.0°C. The surface center is used as the reference at all heights. For clarity, data are plotted only every 6 h.

Figure 6 shows the azimuthal-mean vertical velocity (using the surface center at all heights), averaged (using 6-min data) over each of the same 12-h periods shown in Fig. 5. Similar to NOFLOW, during intensification, eye descent tends to be strongest near 12–13-km height in both sheared simulations. As discussed in Part I, warming itself is at most times not maximized in this region—a consequence of the fact that static stability is very low (about half of that at midlevels).

We note here that the radial distribution of descent is quite sensitive to how the center is defined. In particular, using a (smoothed) geopotential height center that is allowed to vary with height eliminates the zone of strong azimuthal-mean descent at the eye–eyewall interface above 10-km height (not shown). One might expect that such a height-varying center would better reflect the “true” structure, yet a close examination of animations of horizontal cross sections (not shown) reveals that the upper-level vertical velocity field is actually more closely “anchored” to the surface center than it is to the local center. For this reason, we use this height-invariant center for all time-averaged plots.

d. Potential temperature budget in SHEAR5

As discussed in Part I, for moving storms, it is difficult to calculate a budget with acceptable accuracy, as the storm motion itself results in changes in which grid points are used to determine θ (and its changes) between two given times. We have been able to account for this to a certain degree by the following procedure: smooth the storm center position in time (to avoid discrete jumps), calculate the storm motion from the smoothed centers, calculate the horizontal “advection” of θ by the storm motion, and finally subtract this term from the sum of the other tendencies. When using 1-min data, this procedure can (at times) greatly reduce the error in the θ budget (not shown).

Figure 7 shows the tendencies on θ from total advection, diabatic heating, the PBL parameterization, and horizontal diffusion for two 12-h periods in SHEAR5: one at the start of RI (0000–1200 UTC day 2), and one near the end of RI (0000–1200 UTC day 3). These can be compared to Figs. 7a–d and 7i–l of Part I. Figure 8 shows the contribution to total advection from mean vertical, mean radial, eddy vertical, and eddy radial advection (including storm motion) for these same two periods (cf. Fig. 8 of Part I). At the start of RI, the most obvious difference as compared to the same period in NOFLOW is that in SHEAR5, significant diabatic heating extends much farther inward (Fig. 7b), practically to the center. As in NOFLOW, heating in the developing eyewall is nearly completely offset by (primarily vertical) advective cooling (Figs. 7a, 8b), and as the storm is still relatively

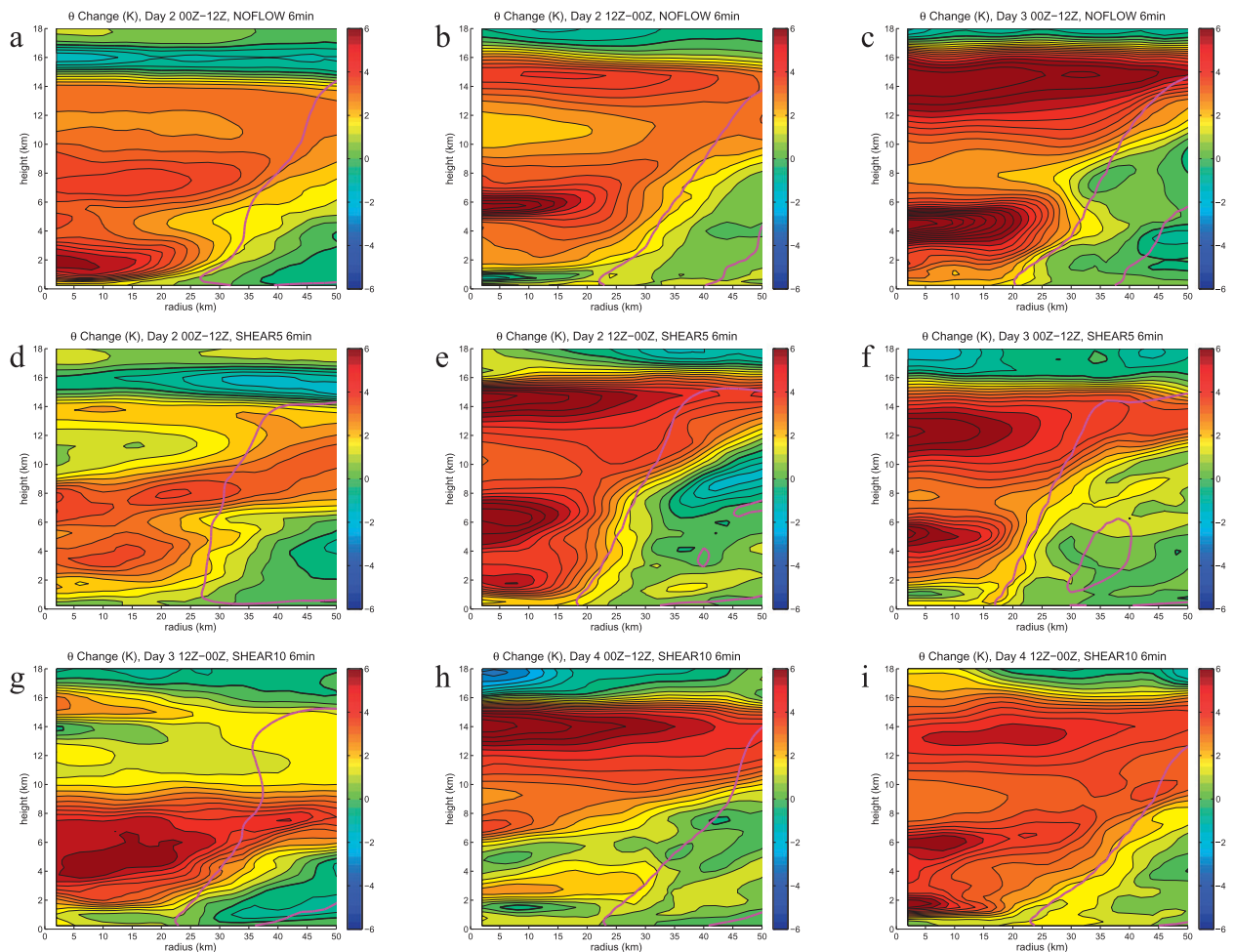


FIG. 5. Plots of 12-h changes in azimuthal-mean potential temperature for consecutive 12-h periods beginning on 0000 UTC day 2 for (a)–(c) NOFLOW and (d)–(f) SHEAR5, and (g)–(i) 1200 UTC day 3 for SHEAR10. Contours are every 0.5°C from -10.0° to $+10.0^{\circ}\text{C}$ (colorbar from -6.0° to $+6.0^{\circ}\text{C}$), with the zero contour thickened. The 12-h mean $+0.10\text{ m s}^{-1}$ azimuthal-mean vertical velocity is contoured in magenta. Note that the radial scale has been restricted to the inner 50 km, so as to focus on the eye. The surface center is used at all heights.

weak, the net change in θ is determined by the small difference between these two very large terms [the maximum of each is on the order of 100 K (12 h)^{-1}]. Much of the nascent eye below 10-km height actually experiences mean ascent at this time (Fig. 6d) and, therefore, a cooling tendency. As in NOFLOW, eddy radial advection is a major contributor to the warming of the midlevel eye at this time (Fig. 8c).

By the start of day 3, the storm in SHEAR5 is already quite intense (Fig. 2a), with $V_{\text{max}10}$ exceeding 50 m s^{-1} , though RI continues for another 12 h. A well-defined eye now exists, and the two maxima in eye warming (at 5- and 12-km height; Fig. 5f) are primarily due to mean vertical advection (Fig. 8f). The minimum in net warming (Fig. 5f) corresponds with a region of ascent (Fig. 6f) and mean vertical advective cooling (Fig. 8f). Descent near

the center at 12 km is nearly 3 times larger than at 5 km, though the net warming is nearly the same. This is (as discussed in Part I) because static stability is very small in the upper troposphere (about 3 times smaller than at 5 km; not shown). The main difference in the budget from 24 h prior is that now that the storm is intense, there is a radially narrow zone of strong diabatic cooling just inward of the eyewall (Fig. 7f) and a broader zone of strong cooling from horizontal diffusion extending inwards from the eye–eyewall interface to very near the center (Fig. 7h). It is largely these two terms that prevent the concentrated zone of descent along the interface from resulting in a very large net warming. This increase in the importance of horizontal diffusion with intensity is consistent with the results from Part I. Overall, the mechanisms contributing to the warming of the eye in

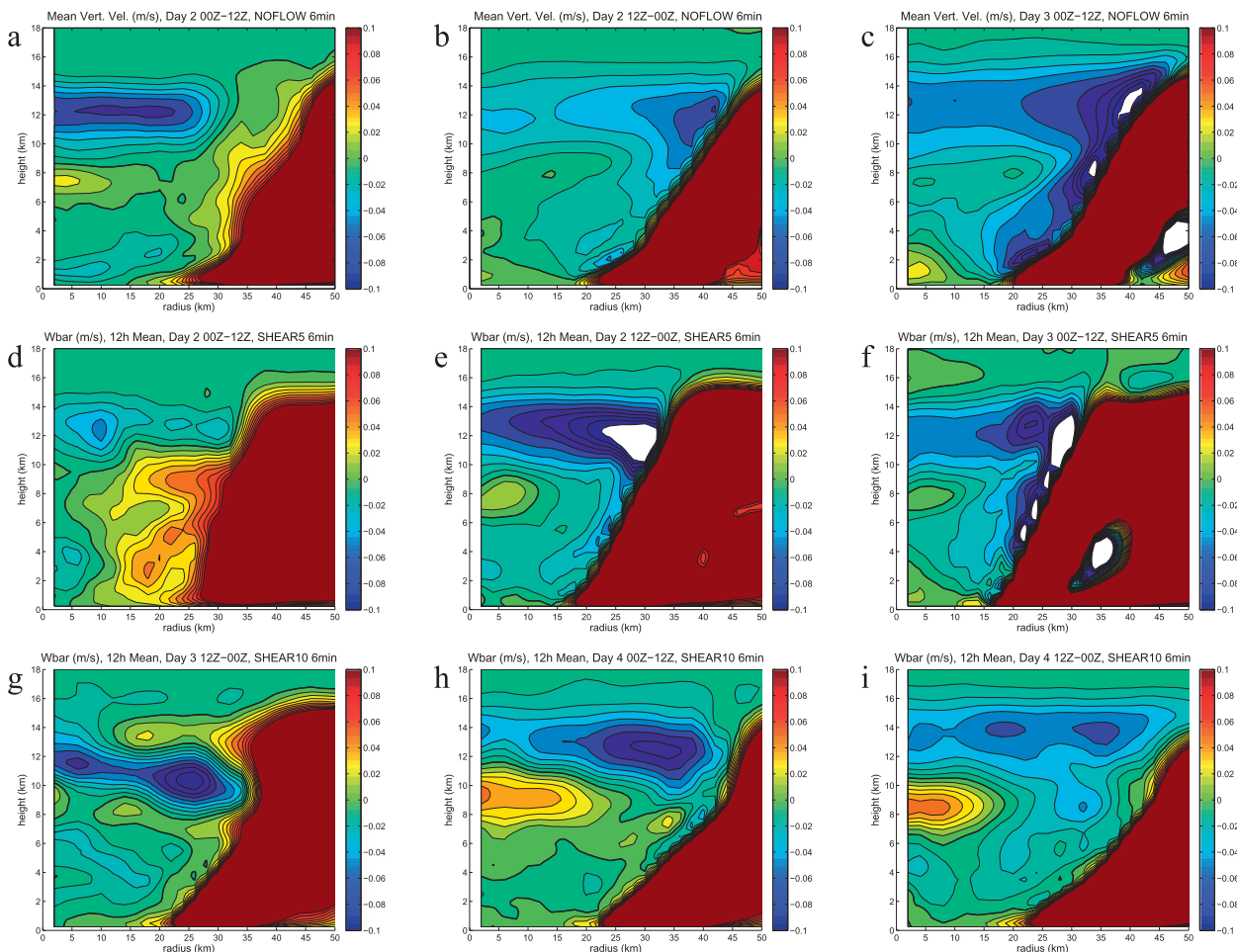


FIG. 6. As in Fig. 5, but for azimuthal-mean vertical velocity, contoured every 0.01 m s^{-1} from -0.1 to $+0.1 \text{ m s}^{-1}$. The zero contour is thickened.

intensifying tropical cyclones are similar, both with and without vertical wind shear.

3. Trajectory analysis

a. Previous studies

In Part I, we have seen that a potential temperature budget is useful for understanding the mechanisms that lead to the warming of the eye. A complementary perspective can be gained from a trajectory analysis, which provides local and Lagrangian information on the history and evolution of the individual parcels that make up the eye. There are a few recent studies that have undertaken such an analysis in tropical cyclone simulations. As part of their multipart study of Hurricane Andrew (1992), Liu et al. (1999) calculated trajectories with hourly model output from a simulation with 6-km horizontal grid spacing. They presented a single backward trajectory, ending at the storm center at 3.2-km

height, and found that this parcel originated at 7.5-km height 32 h earlier.⁴ From this, they concluded that most air in the eye has a very long residence time. This was also the view of Willoughby (1998), who came to that conclusion based on examining the thermodynamic properties of observed eye soundings. Note that Willoughby (1998) found that it was implausible for eye parcels in low levels to have descended within the eye from near the tropopause, while Liu et al. (1999) explicitly state (but never show) that parcels near the eye–eyewall interface descend through the depth of the troposphere.

⁴ The text of Liu et al. (1999) gives the mean descent as 6.5 cm s^{-1} and an origination height of 10.5 km, but their Fig. 6c (and its caption) indicates an origination height of 7.5 km, initially rising to 10.5 km after a few hours before descending. Therefore, the mean descent over the period given is 3.7 cm s^{-1} . It should be noted that the use of hourly data in this trajectory calculation renders the results likely unreliable.

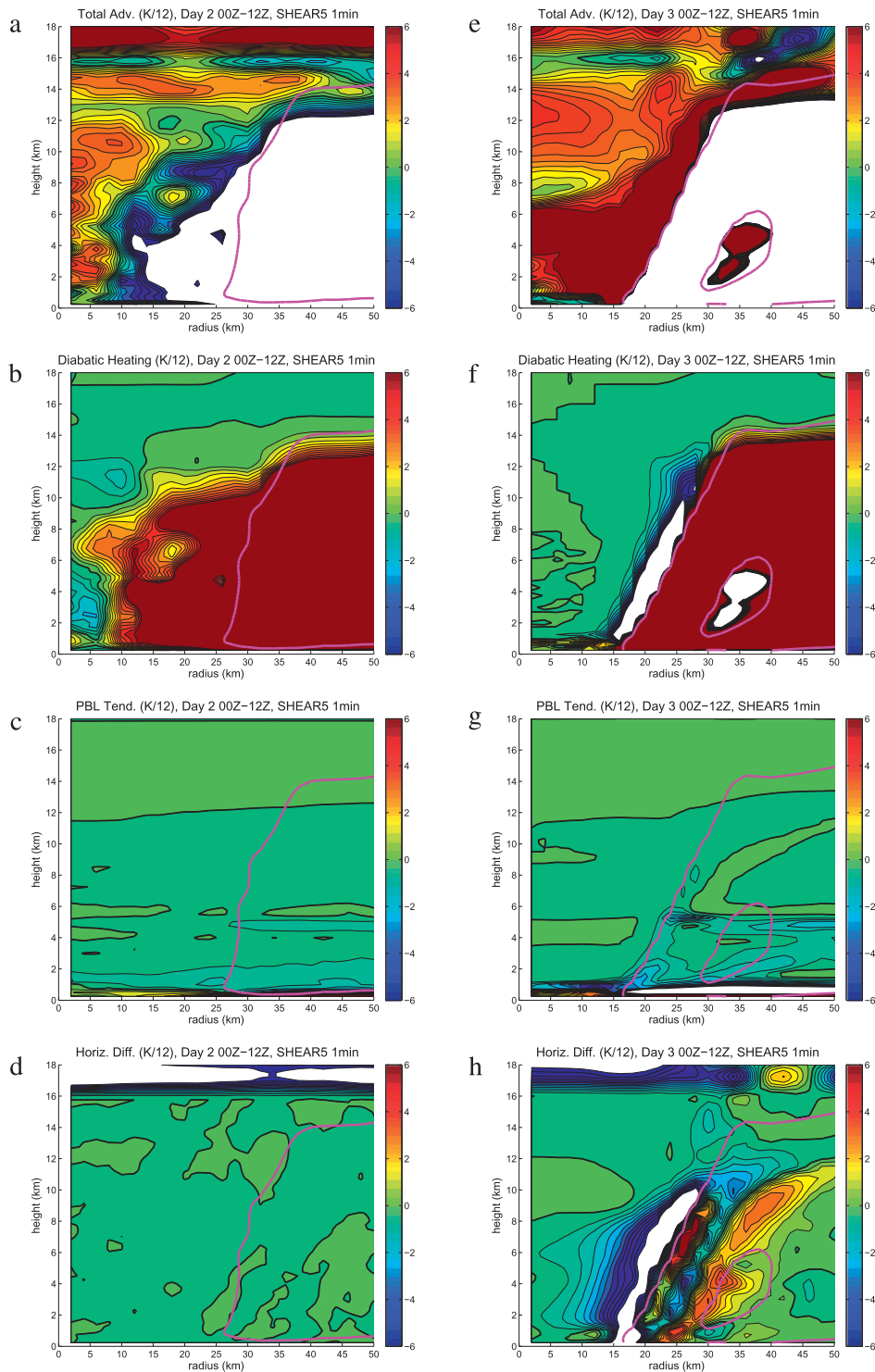


FIG. 7. For SHEAR5, (top)–(bottom) the tendency (using 1-min data) on azimuthal-mean θ from total advection (TADV), diabatic heating (HEAT), the PBL scheme including vertical diffusion (PBL), and horizontal diffusion including Rayleigh damping (HDIF). Each field is contoured from -6.0 to $+6.0$ $\text{K} (12 \text{ h})^{-1}$, every 0.5 $\text{K} (12 \text{ h})^{-1}$. The zero contour is thickened, and in each panel, the $+0.10$ m s^{-1} contour of (time averaged) azimuthal-mean vertical velocity is in magenta. These fields are shown for (left) 0000–12000 UTC day 2 and (right) 0000–12000 UTC day 3.

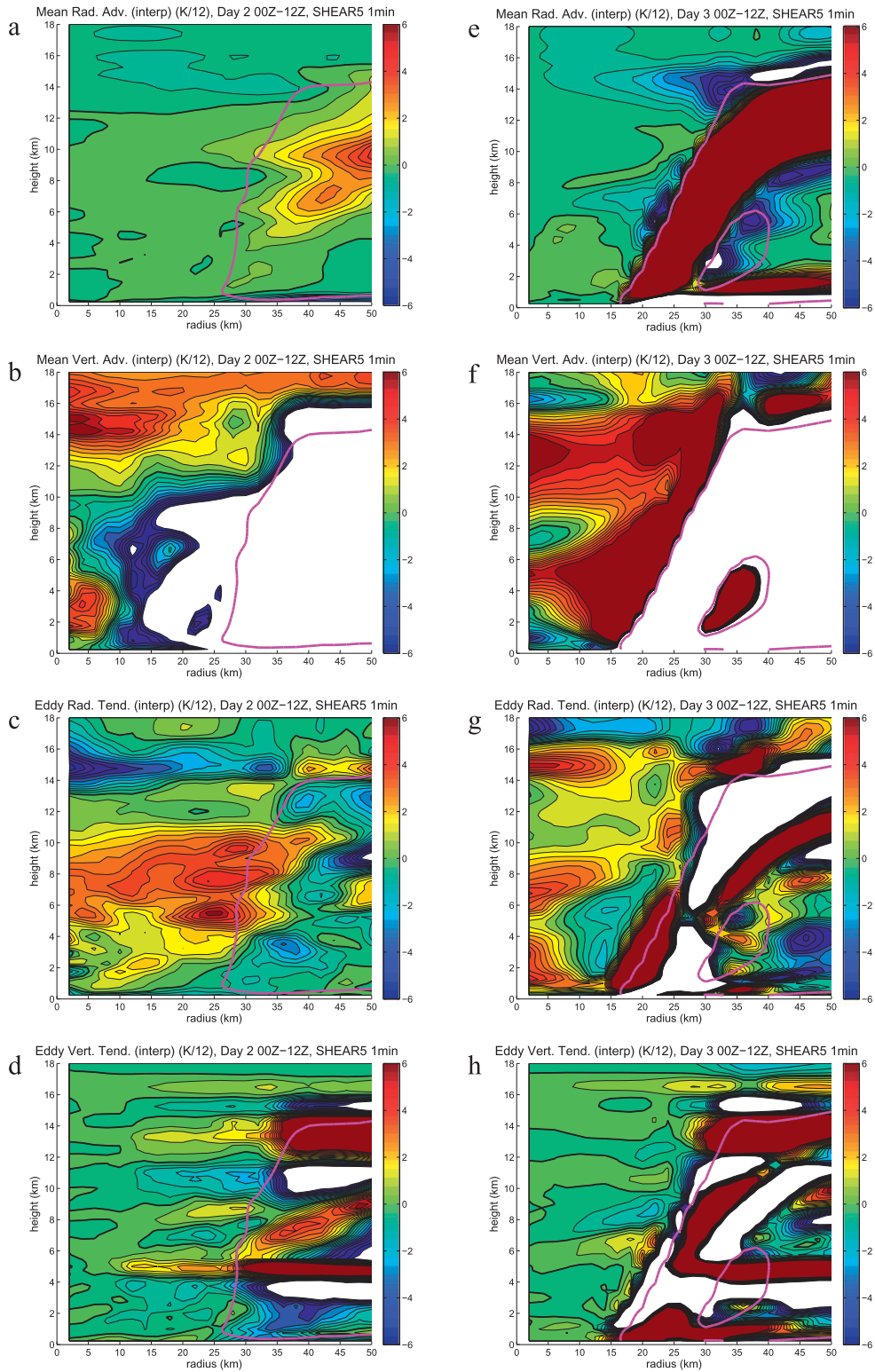


FIG. 8. As in Fig. 7, but for the decomposition of total advection into (top)–(bottom) the tendency from azimuthal-mean radial advection (RADVM), azimuthal-mean vertical advection (VADVM), eddy radial advection (RADVE), and eddy vertical advection (VADVE). Note that RADVM here includes the contribution from storm motion.

Cram et al. (2007) investigated the high-resolution (2 km) simulation of Hurricane Bonnie (1998) of Braun et al. (2006). Cram et al. (2007) used 5 h of model output at 3-min intervals to calculate several thousand trajectories at various locations within the storm. They found that for trajectories initiated in the low-level eye (~450-m height, inside a radius of 24 km), 57% were entrained into the eyewall within 5 h. For trajectories initiated in the eye at 5.6- and 9.8-km height, 59% and 76% were entrained into the eyewall, respectively. The results of Cram et al. (2007) are in apparent disagreement with Liu et al. (1999) and Willoughby (1998), in that the residence time of parcels in the mid- and upper-level eye in the simulated Bonnie was rather short. However, as discussed in Cram et al. (2007), Bonnie was under the influence of relatively strong vertical wind shear, and this may have led to enhanced stirring between the eye and eyewall.

There remains much uncertainty regarding the residence time of parcels in the eye above the boundary layer and the degree to which stirring between the eye and eyewall occurs. Further, the source of parcels that make up the strongest part of the warm core is unclear. Here, using simulations in both quiescent and sheared environments, we calculate trajectories in order to partially address these questions.

We use the postprocessing software RIP4 (Stoelinga 2009) to calculate both forward and backward trajectories from model output at either 1- or 6-min intervals, using a 10-s trajectory time step. The 6-min data is used for certain trajectories because of limitations on storage capacity. We have carefully examined the sensitivity to sampling interval by comparing 6- to 1-min trajectories for select 12-h periods within both NOFLOW and SHEAR5 (not shown). While the 6-min trajectories are not identical to the 1-min trajectories, they are generally qualitatively very similar to each other. Although there are some noticeable differences in trajectory behavior for parcels that approach the eye–eyewall interface at midlevels, overall the differences remain small. Further, none of the results that follow are meaningfully different between using 6- and 1-min data. The fact that 1- and 6-min trajectories are very similar to each other in a statistical sense makes us confident that the calculations are generally converged at these sampling frequencies, and so we believe the trajectories to be sufficiently accurate.

b. 12-h backward trajectories ending in the eye

First, to investigate the source of air in the eye during RI, we calculate 12-h backward trajectories (using 1-min data) for parcels that end within the eye. Specifically, at a given height, we seed [to use the terminology of Cram et al. (2007)] the trajectories at each gridpoint that is found within 15 km of the center. Figure 9 shows a radius–height

view of the path of these 177 trajectories for NOFLOW; for seed heights of 2, 6, and 10 km; and for ending⁵ times of 1200 UTC day 2, 0000 UTC day 3, and 1200 UTC day 3. The source regions of parcels in the eye are quite different for the first 12-h period as compared to the latter two periods. Looking first at 2 km ending at 1200 UTC day 2 (Fig. 9a), a large number of eye parcels originate (12 h earlier) within the boundary layer inflow, well outside the nascent eyewall. There are a smaller number of parcels that have been within the eye for the entire 12-h period, and most of these originate between 3- and 4-km heights. For the trajectories ending at 2 km at 0000 UTC day 3 (Fig. 9d) and at 1200 UTC day 3 (Fig. 9g), there is a very different distribution: the vast majority of eye parcels originate within the eye, and only a few have been in the inflow layer in the previous 12 h. Although still within the confines of the eye, many trajectories for the middle period originate from outside 20-km radius, and have moved substantially inward over this period. Therefore, while there may not be much stirring between the eye and eyewall at this time in NOFLOW, there is stirring within the eye.

At 6-km height, the contrast between backward trajectories ending at 1200 UTC day 2 (Fig. 9b) and those at 0000 UTC (Fig. 9e) and 1200 UTC (Fig. 9h) day 3 is even more stark. For the first period, the mean eyewall updraft is clearly traced out by many of the trajectories, and the origin of these trajectories 12 h previously is either within the eyewall or within the boundary layer inflow. For trajectories ending at 0000 and 1200 UTC day 3, however, virtually all originate in the eye near 7-km height. At 10 km, the behavior of the trajectories is more similar between these three periods than it is at the lower heights, as all of the eye parcels at all three times have remained within the eye for the entire 12-h period (Figs. 9c,f,i).

In the sheared simulations, the storm center can tilt with height considerably when the storm is weak (Fig. 3). Therefore, we seed backward trajectories in these simulations based on the storm center location at the height at which the trajectories are initialized, and the time evolution of the radius of the trajectories is calculated with respect to this center as well. For 5 m s^{-1} of shear, the behavior of the backward trajectories is qualitatively similar to NOFLOW (Fig. 10). For the first 12-h period (ending at 1200 UTC day 2), the vast majority of parcels ending at 2-km height in the eye originate either within

⁵ For clarity, “beginning” and “ending” times refer to the chronologically earlier and later of the two times that bound the trajectory, respectively, whether the trajectory is forward or backward.

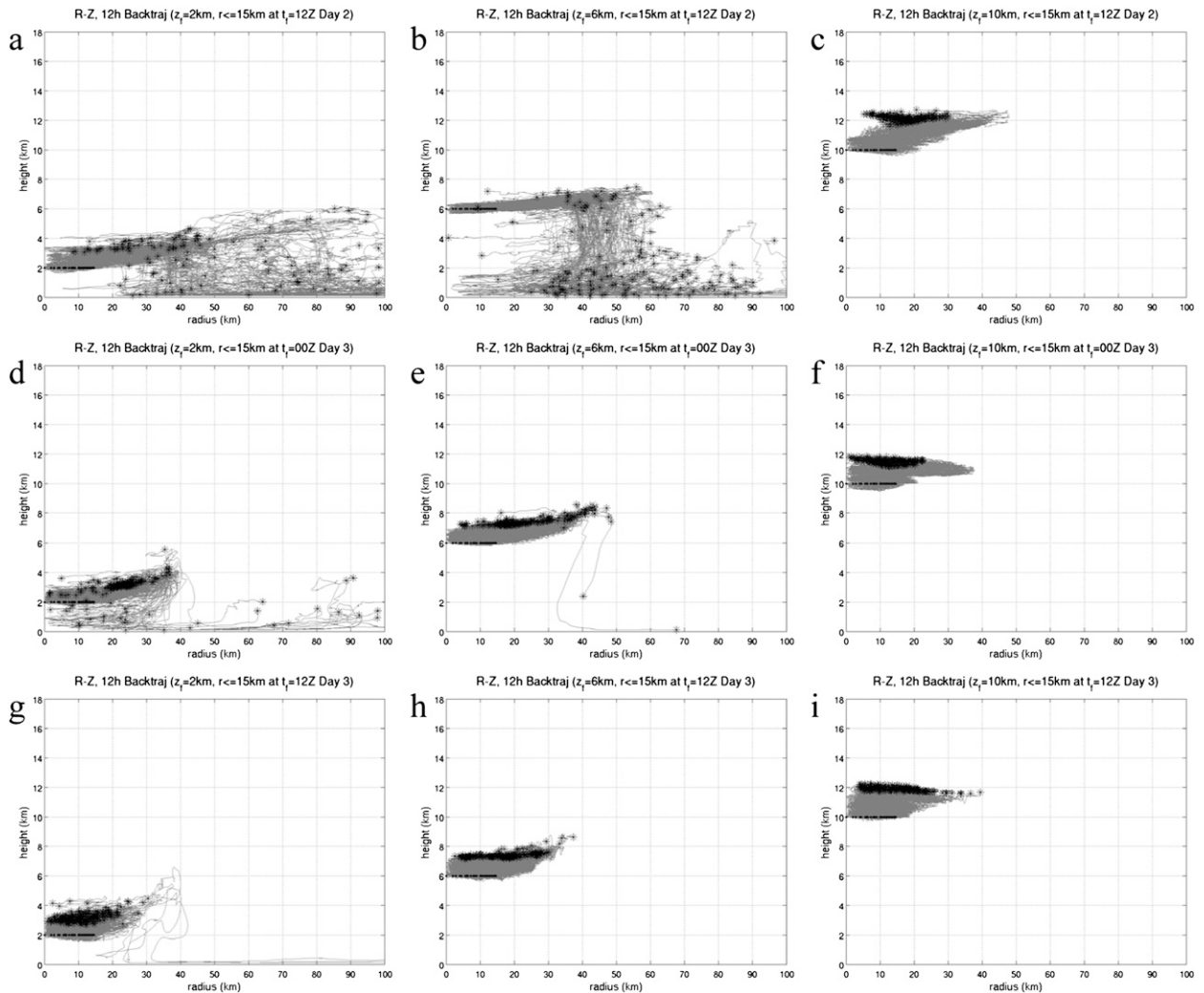


FIG. 9. Radius–height views of 12-h back trajectories in NOFLOW that end within 15 km of the center at (a)–(c) 1200 UTC day 2, (d)–(f) 0000 UTC day 3, and (g)–(h) 1200 UTC day 3, at heights of (left) 2, (middle) 6, and (right) 10 km. There are 177 trajectories in each panel. The starting and ending points of the trajectories are indicated by black asterisks and dots, respectively.

the boundary layer inflow or within the developing low-level eyewall, outside 30-km radius. Fewer parcels originate within or outside the eyewall for the period ending at 0000 UTC day 3, and almost none do for the period ending at 1200 UTC day 3. The reduced eye–eyewall stirring with increasing intensity is again evident at 6 and 10 km, although many parcels still originate outside the eye at these heights for the period ending at 0000 UTC day 3, unlike in NOFLOW. Since SHEAR5 and NOFLOW exhibit nearly identical intensity evolution during these periods (Fig. 2), the trajectory comparison is a measure of the direct effect of shear. For this magnitude of shear, it appears that this class of trajectories is perhaps somewhat altered, although not to a substantial degree.

As the onset of RI is delayed in SHEAR10 because of the stronger shear, we compare this simulation to the others at times corresponding to similar intensities by examining backward trajectories that end at 0000 UTC day 4, 1200 UTC day 4, and 0000 UTC day 5 (Fig. 11). Because of storage considerations, we compute all trajectories for SHEAR10 using 6-min data. Here, the effect of shear is somewhat more evident, at least at upper levels. Despite actually being slightly more intense during the first 12-h period, most parcels ending at 10-km height originate far from the storm center, and this remains the case during the subsequent 12-h period as well. Only after $V_{\max 10}$ exceeds about 60 m s^{-1} do the backward trajectories mostly originate within the eye. A closer examination of these trajectories reveals that

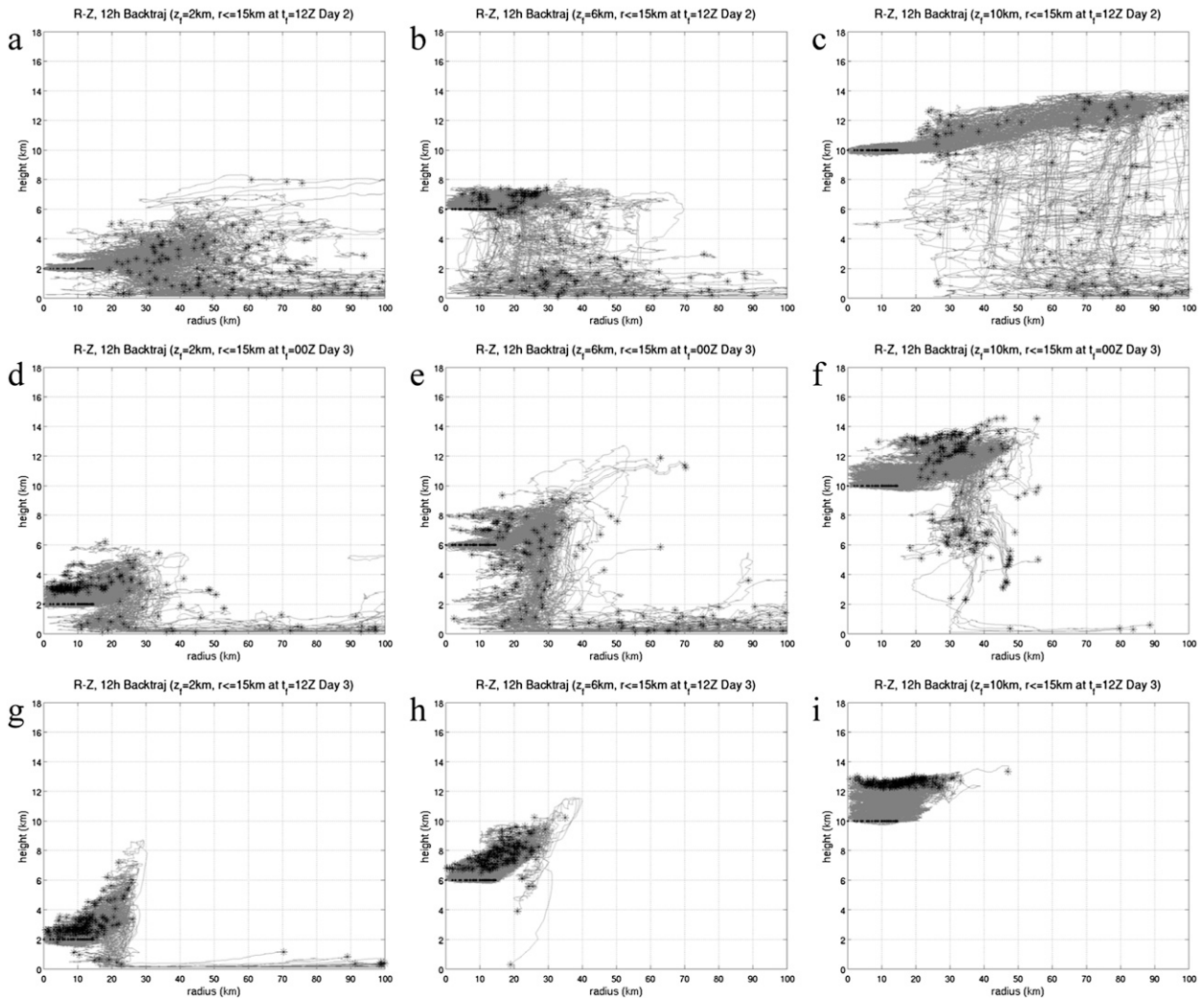


FIG. 10. As in Fig. 9, but for SHEAR5.

during the first two periods, even the parcels that begin and end close to the center at some point exceed the radius of the eyewall, with the majority of them exceeding 100-km radius. In other words, almost all parcels ending near the center at upper levels have indeed recently been found outside the eye. Therefore, for a large enough magnitude, shear can actually have a substantial direct effect on the behavior of trajectories in the eye. The dominant influence of intensity remains, however, as the stirring between the center of the eye and eyewall is greatly reduced once a sufficient intensity is reached.

c. 12-h forward trajectories beginning in the eye

To further illustrate how the residence time of air in the midlevel eye changes dramatically as the storm intensifies, Fig. 12 shows, for NOFLOW, histograms of the

ending radii and heights for parcels that originate at 6-km height and within 15 km of the center, for forward trajectories initiated at six different times, every 2 h from 0100 UTC to 1100 UTC day 2. A striking change in behavior is evident between 0300 and 0700 UTC. For trajectories starting at 0300 UTC (Fig. 12b), 92 out of 177 (52.0%) are found outside 100-km radius after 12 h, and only 28 out of 177 (15.8%) are found inside 35-km radius (the approximate inner edge of the eyewall at 6-km height). For trajectories initiated only 2 h later (0500 UTC) (Fig. 12c), the number of parcels remaining inside 35 km after 12 h nearly doubles (31.1%). Two peaks are seen in the distribution of ending heights (Fig. 12i)—one from 12 to 15 km (the outflow layer), and the other from 5 to 6 km, representing the parcels that remained inside the eye and descended. For trajectories initiated at 0700 UTC (Fig. 12d), nearly all of the parcels

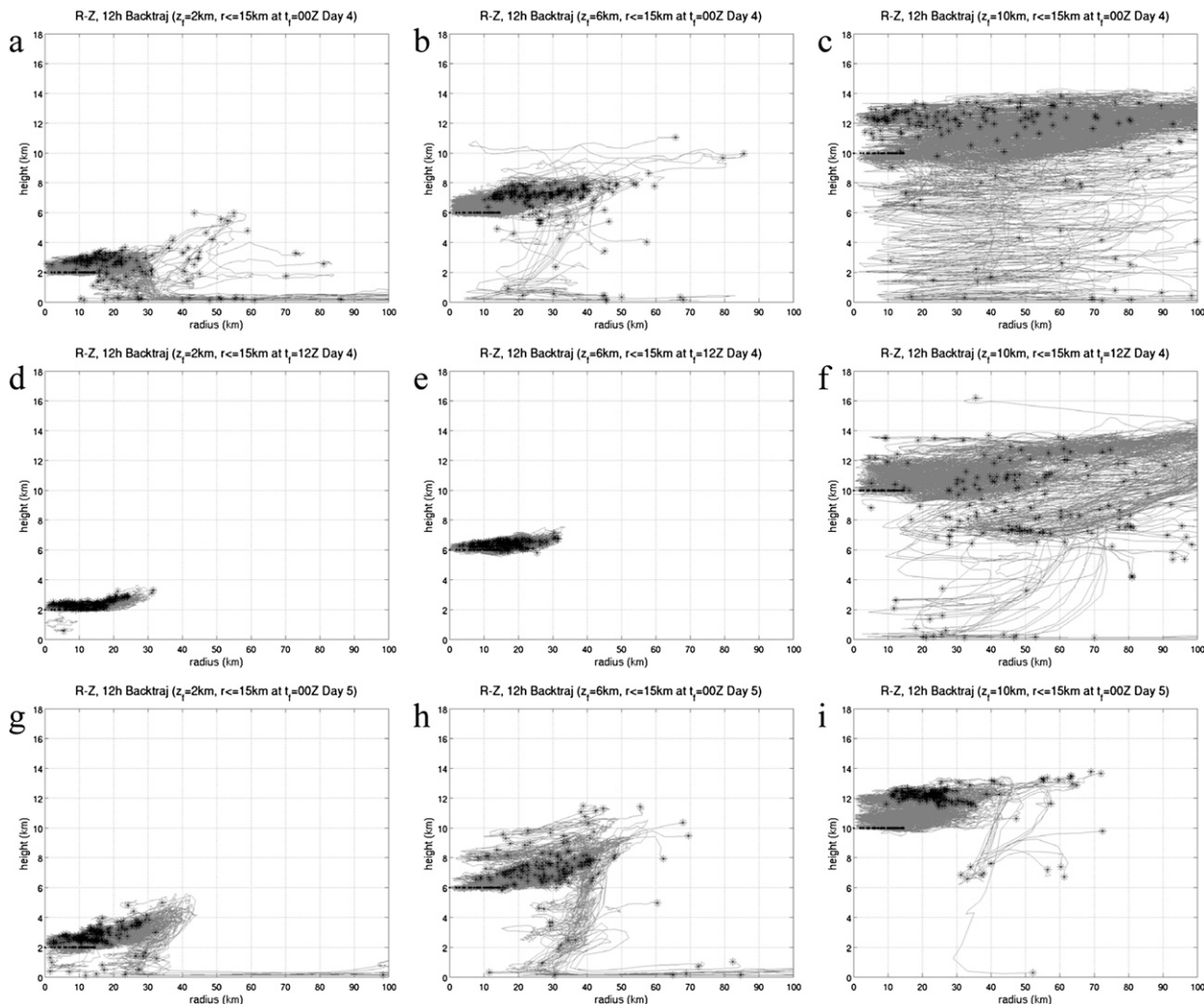


FIG. 11. As in Fig. 9, but for SHEAR10. The times chosen for these trajectories are offset by 36 h from those used for the other simulations (see text). Note that for these trajectories, 6-min data are used.

remain inside 35 km (89.8%). A pronounced peak in the heights is seen for 5.25–5.50 km (Fig. 12j), indicating that the most common fate for a parcel initially in the eye at this time is to descend by 500–750 m over the following 12 h. Nevertheless, there are some parcels that descend by almost 3 km. As we discuss below, there are some subsequent periods of increased mixing, as is evident for trajectories initiated at 1100 UTC (Fig. 12f). Nevertheless, the forward trajectories are consistent overall with the backward trajectories, in that they both indicate less stirring between the eye and eyewall (and an increased residence time for parcels within the eye) once the storm intensifies beyond a certain point.

Just as in NOFLOW, in each of the sheared simulations, there is a rapid change with intensity in the behavior of forward trajectories initiated inside the eye. To

compare the three simulations, Figs. 13a and 13b show time series of the percentage of parcels originating inside 15-km radius at 6-km height that after 12 h are found inside 35 km and outside 100 km, respectively. Each time shown is the starting time of a different set of trajectories, from 0000 UTC day 1 to 1200 UTC day 7. To investigate the evolution over the entire simulation, these trajectories utilize 6-min data (we have confirmed that this frequency is sufficient for this purpose by comparing to 1-min data over select 12-h periods). For both NOFLOW and SHEAR5, there is a rapid increase in parcels remaining inside the eye (i.e., decreased stirring) as the initiation time increases from 0000 to 0800 UTC day 2. However, it is now also apparent that the degree of stirring thereafter increases systematically with initiation time until 1700 UTC day 2, before once again decreasing

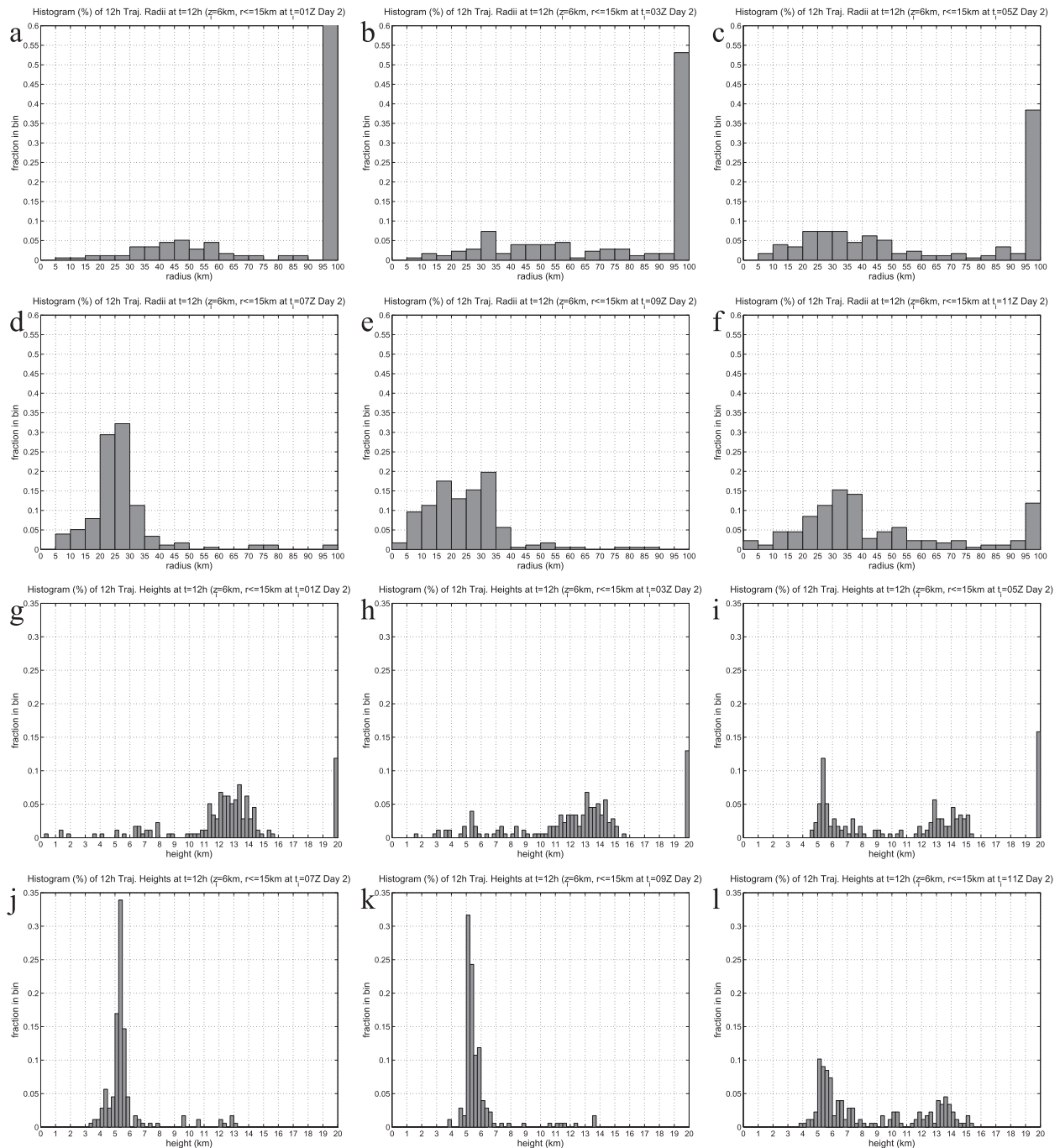


FIG. 12. For NOFLOW, histograms of (a)–(f) the ending radii and (g)–(i) the heights for 12-h forward trajectories originating at 6-km height and within 15 km of the center, at 2-h intervals, from 0100 to 1100 UTC on day 2. The bin width is 5 km for radius and 0.25 km for height. All trajectories that end at radii larger than 100 km or that exit the domain are assigned to the 95–100-km-radius bin. All trajectories that exit the domain are assigned to the 19.75–20.00-km bin.

rapidly. Somewhat remarkably, SHEAR5 exhibits nearly identical behavior to NOFLOW, with the maxima and minima in stirring occurring at approximately the same times in both simulations. At all times after 2000 UTC day 2, nearly all parcels initiated inside the

eye remain there after 12 h, for both NOFLOW and SHEAR5.

Even under 10 m s^{-1} of shear, once a sufficient intensity is achieved, stirring of the midlevel eye becomes greatly suppressed. For trajectories initiated prior to

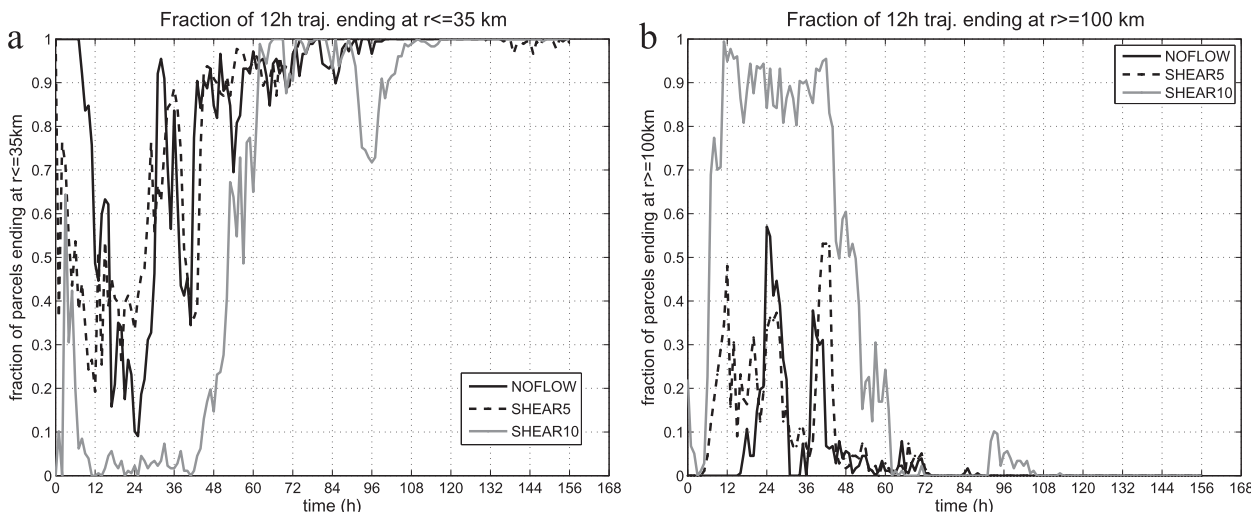


FIG. 13. Time series of the percentage of parcels that after 12 h are found (a) inside 35-km radius and (b) outside 100-km radius. Each time (every hour) is the starting time of a different set of forward trajectories, using 6-min data.

1700 UTC day 2, nearly all parcels are stirred out of the eye within 12 h in SHEAR10. Thereafter, there is a rapid increase in the percentage of parcels remaining inside the eye, nearly coincident with the beginning of RI. At most times after 1400 UTC day 3, nearly all 12-h trajectories remain inside the eye. It is clear that the delay in the reduction of stirring in SHEAR10 relative to the other simulations is related to the delay in the onset of RI, which is further evidence of the dominant effect of intensity on the behavior of eye trajectories.

d. The fate of parcels along the eye–eyewall interface

In Part I, we showed that the maximum azimuthal-mean descent tends to be concentrated in a radially narrow zone along the eye–eyewall interface. In all simulations, this zone tends to have two maxima,⁶ near 14- and 2-km heights, with time-mean magnitudes as large as 10–20 cm s⁻¹—much greater than is found at the center of the eye (Fig. 6; cf. Fig. 9 of Part I). How far parcels in this interface region are actually able to descend before being entrained into the eyewall updraft, or perhaps moving farther into the eye away from the region of large descent, is currently unknown.

To ascertain the fate of parcels in the zone of maximum descent, we compute 12-h forward trajectories initiated at 0000 UTC day 6 at 14-km height, seeded in the 40–50-km radius annulus for NOFLOW and in the 46–56-km annulus for SHEAR5. Figure 14 shows the

(Earth relative) horizontal and radius–height views for these trajectories in NOFLOW, as well as time series of vertical velocity w and θ . In NOFLOW, the instantaneous mean vertical velocity over all 716 trajectories at the starting time is -13.7 cm s^{-1} , but ranges from -7.8 to 4.7 m s^{-1} . For the 608 parcels (84.9%) that undergo net descent during this 12-h period, the mean final height is 12.1 km, or a mean vertical velocity of -4.46 cm s^{-1} . The lowest final height of any trajectory is 10.8 km, or a mean vertical velocity of -7.27 cm s^{-1} . This particular trajectory happened to have an initial w of $+1.13 \text{ m s}^{-1}$, perhaps indicating that the instantaneous vertical velocity is not a good predictor of whether a parcel will undergo net descent over a longer period. The lack of any such relationship is confirmed by examining scatterplots of initial w versus net displacement (not shown).

As the zone of maximum descent is collocated with an axis of azimuthal-mean inflow, parcels in this region (in NOFLOW) generally move inwards as they descend along the sloping eye–eyewall interface, and so most of them remain inside the encroaching eyewall [consistent with the conclusions of Willoughby (1998)]. In fact, it is clear that there is actually a tendency for parcels to systematically move inwards relative to the radius of the eyewall, such that they eventually are advected away from the zone of maximum descent. This indicates that at least to a certain degree, the strong descent along the eye–eyewall interface does influence the composition and thermodynamic budget of air farther inside the eye. On the other hand, while many of these parcels have moved 10–15 km inward in 12 h, they will likely take substantially longer to approach the center, as the mean radial velocity is very small inward of the interface. It is

⁶ As discussed in section 2c, the upper-level maximum is not present when averaging with respect to a center that is allowed to vary with height.

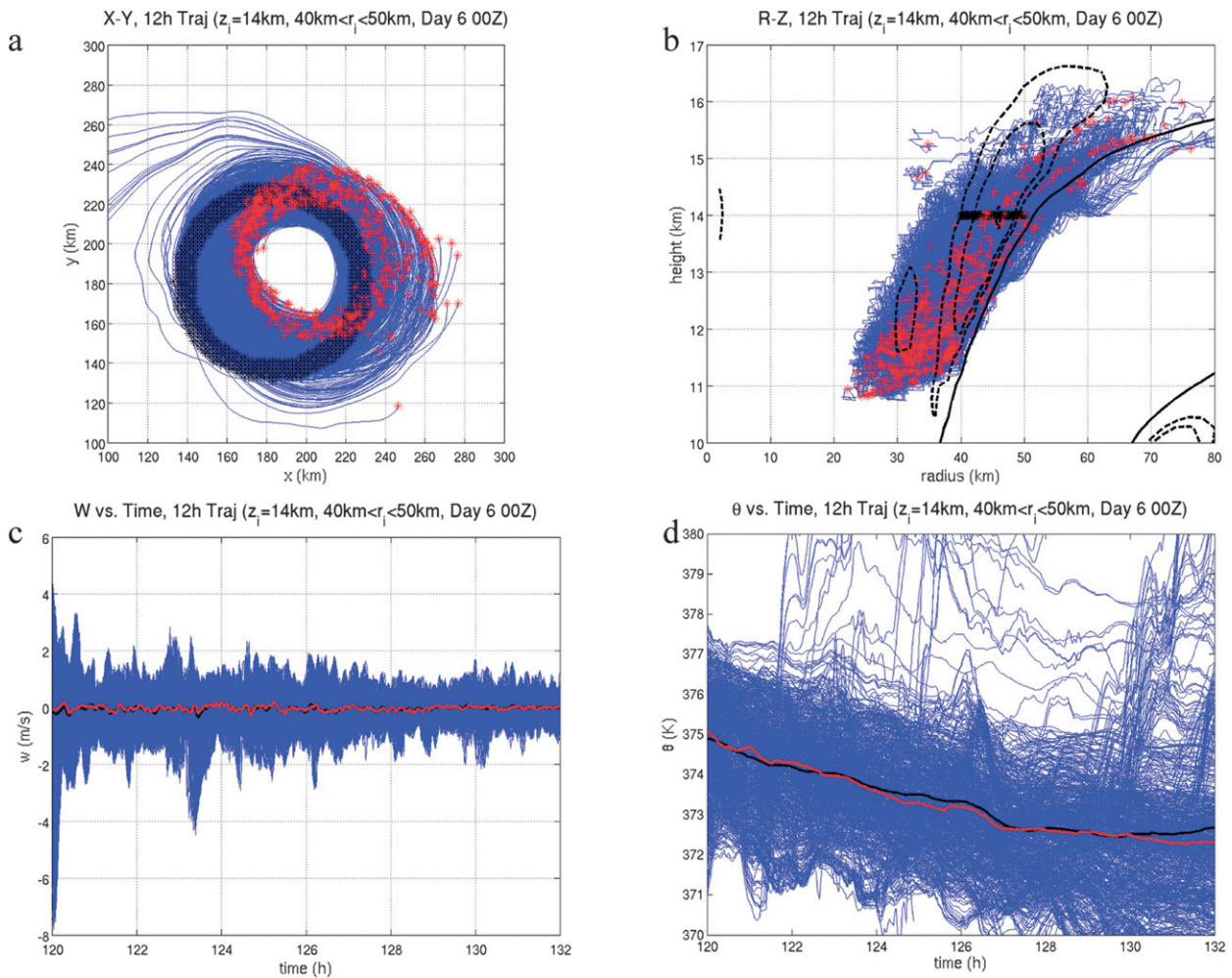


FIG. 14. For NOFLOW, 12-h forward trajectories (using 1-min data) initiated at 0000 UTC day 6 at 14-km height, seeded in the annulus from 40- to 50-km radius (716 trajectories). (a) Horizontal and (b) radius–height views of the trajectories. Time series of (c) vertical velocity and (d) θ , along the trajectories. In (a),(b), the initial and final locations of each trajectory are indicated by the black and red asterisks, respectively. In (c),(d), the mean and the median over all (existing) trajectories are given by the black and red lines, respectively. Also drawn in (b) are the $+10 \text{ cm s}^{-1}$ (solid black) and the -2.5 , -5 , and -10 cm s^{-1} (dashed black) contours of azimuthal-mean vertical velocity.

clear from the time series (Fig. 13d) that θ decreases (by a median value of 2.8 K) as the parcels descend, presumably the result of a combination of horizontal diffusion and sublimative cooling (cf. Figs. 6q,s of Part I). The average rate of cooling from the sum of these two terms (at $z = 14 \text{ km}$ and from $r = 40$ to 50 km) is $-1.7 \text{ K (12 h)}^{-1}$, and so the behavior of the trajectories is qualitatively consistent with our budget in Part I.

We have also computed analogous trajectories in NOFLOW at 0000 UTC day 3 for comparison (not shown). There are some notable differences. On day 3, some parcels are able to descend by 4–7 km, whereas on day 6, no parcels descend by more than 3 km. Another difference is that some parcels on day 3 are able to move much farther inward, and reach the center within 12 h.

Finally, a somewhat greater fraction of parcels initiated along the eye–eyewall interface on day 3 end up being entrained into the eyewall than on day 6. This enhanced stirring on day 3 relative to day 6 is consistent with the idea that increased intensity and inertial stability (on day 6) leads to a reduction in eye–eyewall stirring. In spite of this greater entrainment on day 3, most parcels (71.6%) still experience net descent over 12 h (not shown). Therefore, at two very different stages of storm evolution, most parcels along the eye–eyewall interface can remain at or inward of the interface for at least 12 h, at least in the absence of shear.

In the presence of vertical wind shear, a rather different picture emerges for the fate of parcels initiated in the upper-level zone of maximum descent (Fig. 15). For

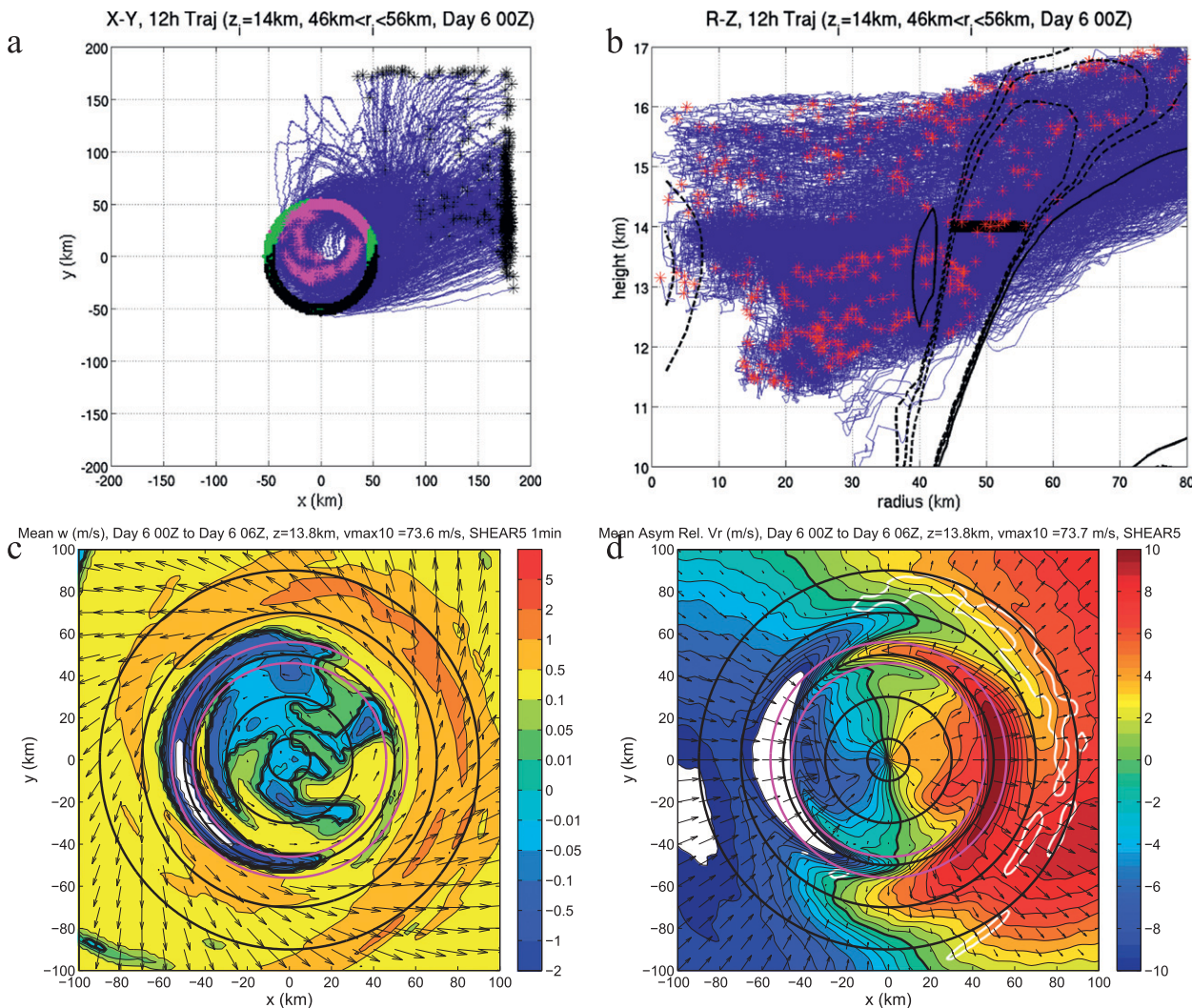


FIG. 15. For SHEAR5, 12-h forward trajectories (using 1-min data) initiated at 0000 UTC day 6 at 14-km height, seeded in the annulus from 46- to 56-km radius (804 trajectories). (a) Horizontal storm-relative and (b) radius–height views of the trajectories. In (a), the initial locations of each trajectory are indicated by dots, with the color indicating whether the trajectories experience net descent (magenta) over 12 h, end more than 100 km from the storm center (black), or neither (green). The magenta and black asterisks indicate the ending points of certain trajectories, with the colors having the same meaning as the dots. In (b), the initial and final locations of each trajectory are indicated by the black and red asterisks, respectively. (c) Storm-centered (sfc center) 6-h composite vertical velocity and (d) storm-relative asymmetric radial velocity, at model half-level 36 (approximately 14-km height) for 0000–0600 UTC day 6. In (c),(d), range rings are in black every 20 km starting at 10 km, and in magenta at 46 and 56 km. In (c),(d), vectors give the storm-relative horizontal flow, and the storm-relative asymmetric radial flow, respectively. In (d), the 1 m s^{-1} vertical velocity contour is in white.

SHEAR5, only 195 out of 804 (24.3%) parcels that are initially found between 46- and 56-km radii at 14-km height undergo net descent over the 12-h period. Of these parcels, 535 (66.5%) and 456 (56.7%) move beyond 75 and 100 km from the center at some point during this period, indicating that most parcels are entrained into the eyewall and outflow layer, primarily in the downshear-left quadrant.

The behavior of the trajectories varies strongly by the initial azimuthal location: Almost all of the parcels that

experience net descent originate in the northeastern quadrant (downshear left), and virtually all parcels that end up more than 100 km from the center after 12 h originate in the southwestern (upshear right) and southeastern (downshear right) quadrants. The parcels initially on the northern side of the storm experience net inward motion as they are advected azimuthally, so that by the time they are to the south of the center, they are only at 20–30-km radius. In contrast, those initially on the southern side of the storm experience net outward motion, so

that they are soon entrained into the eyewall and its much stronger outflow. While some of these parcels are able to be detrained back into the eye once they reach the northern side, most of them are “permanently” displaced downshear of the storm.

Figures 15c and 15d show horizontal cross sections of the 6-h storm-centered mean vertical velocity and storm-relative asymmetric radial velocity at approximately 14-km height, respectively. Unlike in NOFLOW (not shown), in SHEAR5 the zone of strong descent is only found in the upshear semicircle, although where it exists, is quite intense ($< -2 \text{ m s}^{-1}$). It can be seen (Fig. 15a) that the class of parcels that remain within the eye are actually centered more than 90° upstream of the strongest mean descent, and many of the parcels initiated in the zone of descent do not remain within the eye. This is because the fate of the trajectories is largely determined by the radial flow, and there is inflow in the upshear semicircle and outflow in the downshear semicircle (Fig. 15d), and this is consistent with the trajectory behavior.

e. How far can parcels descend within the eye?

The final question we attempt to address with trajectories is how far parcels descend while remaining inside the eye. In particular, can parcels descend through most of the depth of the troposphere, and if so, how long does this process take? To answer these questions, we calculate 4-day (96 h) forward trajectories starting at 0000 UTC day 3, using 6-min output. Figure 16a shows the radius–height view of trajectories in NOFLOW, which originate at the center point at nine different heights between 1 and 16 km, while Fig. 16b shows the time series of the parcels’ vertical displacements. The parcels initially found at 1 and 2 km can only descend by about 500 m but remain inside the eye for over 2 days before entering the eyewall updraft. The parcel initially at 4 km descends by about 3.5 km over 36 h before entering the eyewall, and at 6 km, the parcel descends by less than 2 km and enters the eyewall after just over a day. For 8 km and above, each of the parcels remains within the eye for at least 3 days. During this period, these parcels descend by amounts ranging from 5 to 10 km. For the trajectory seeded at 10 km, the parcel descends in 2 days to a height of about 6 km while remaining near the center of the eye, moves outward to the eye–eyewall interface near 30-km radius, and then descends to nearly the surface over a 12-h period prior to entering the eyewall updraft. The trajectories seeded at 12 and 14 km descend to heights between 4 and 6 km, while remaining within the interior of the eye through the end of trajectory.

It seems clear that in the absence of environmental vertical wind shear, it is indeed possible for parcels to descend through much of the depth of the troposphere

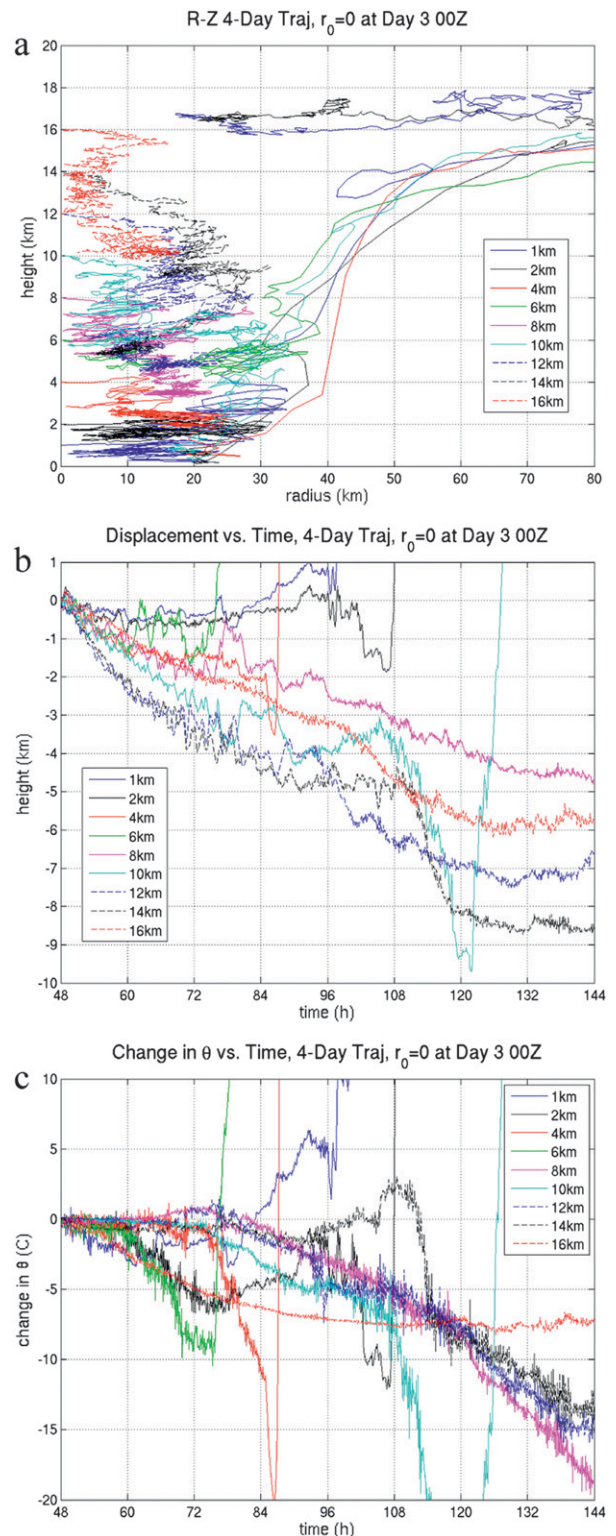


FIG. 16. For NOFLOW, 4-day (96 h) trajectories initiated at 0000 UTC day 3, at the center point at nine different heights between 1 and 16 km. (a) The radius–height view and the time series of (b) vertical displacement and (c) change in θ .

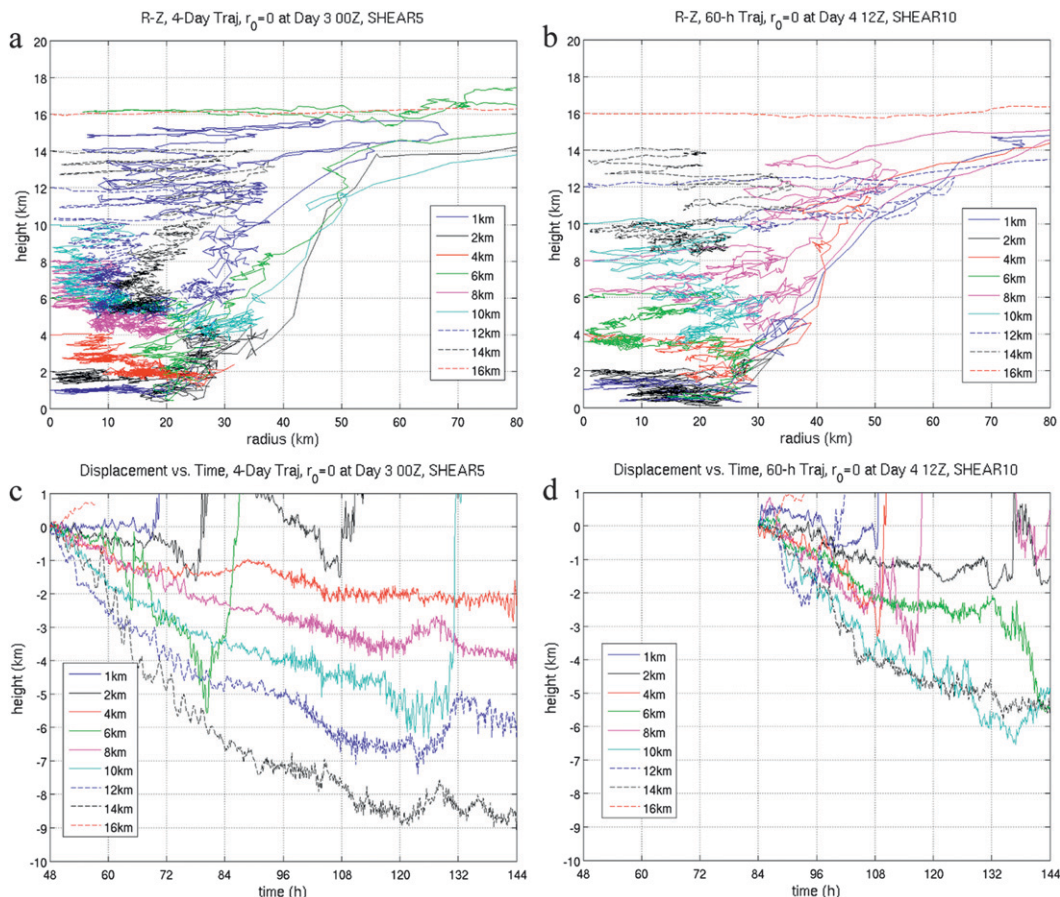


FIG. 17. (a),(b) As in Fig. 16a, but for SHEAR5 and SHEAR10, respectively. In (b), trajectories begin at 1200 UTC day 4, and are only 60 h. (c),(d) As in Fig. 16b, but for SHEAR5 and SHEAR10, respectively.

within the eye. All four of the parcels still within the eye stop descending on day 6, which is consistent with the fact that the mean vertical velocity becomes weak at this time. Figure 16c shows the change in θ versus time for these nine trajectories. For the first 12–36 h, several of these parcels descend substantially while θ changes relatively little, and thereafter θ decreases substantially as they continue to descend (in particular, for the trajectories originating at 8, 12, and 14 km). This explains how parcels can descend great distances without increasing the temperature of the mean vortex to unrealistic values: θ is not always conserved, but rather is generally decreased by horizontal diffusion and (at large enough radii) diabatic cooling. Without interpolating the four-dimensional tendency fields to the trajectories, we cannot directly evaluate the contributions from each term. However, the initial lack of change in θ when the parcels are located near the center above 8 km, followed by large cooling once they have been sufficiently displaced (radially and/or vertically) is qualitatively consistent with the radius–height distribution of diffusive cooling.

While the presence of shear can act to reduce the residence time in the eye, and therefore the net distance that parcels are able to descend while remaining within the eye, overall, the behavior of these “center” trajectories remains qualitatively similar in 5 and even 10 m s^{-1} of shear. Figure 17 shows the radius–height view and time series of vertical displacement for these trajectories in each of the sheared simulations. Trajectories begin at 0000 UTC day 3 in SHEAR5 and at 1200 UTC day 4 in SHEAR10 (so that the initial intensities are comparable), and end at 0000 UTC day 7 in both simulations. As the tilt is relatively small at the start of these trajectories, we use the surface center for these calculations (the results are largely insensitive to this choice). There are two main differences from NOFLOW: at and below 14 km there are larger radial oscillations in the sheared simulations, while the parcels initially at 16-km height are quickly advected away from the storm and exit the domain within 12 h. The first phenomenon is due to fact that with shear the storm-relative radial flow reverses as the parcels orbit the eye, so that outward excursions

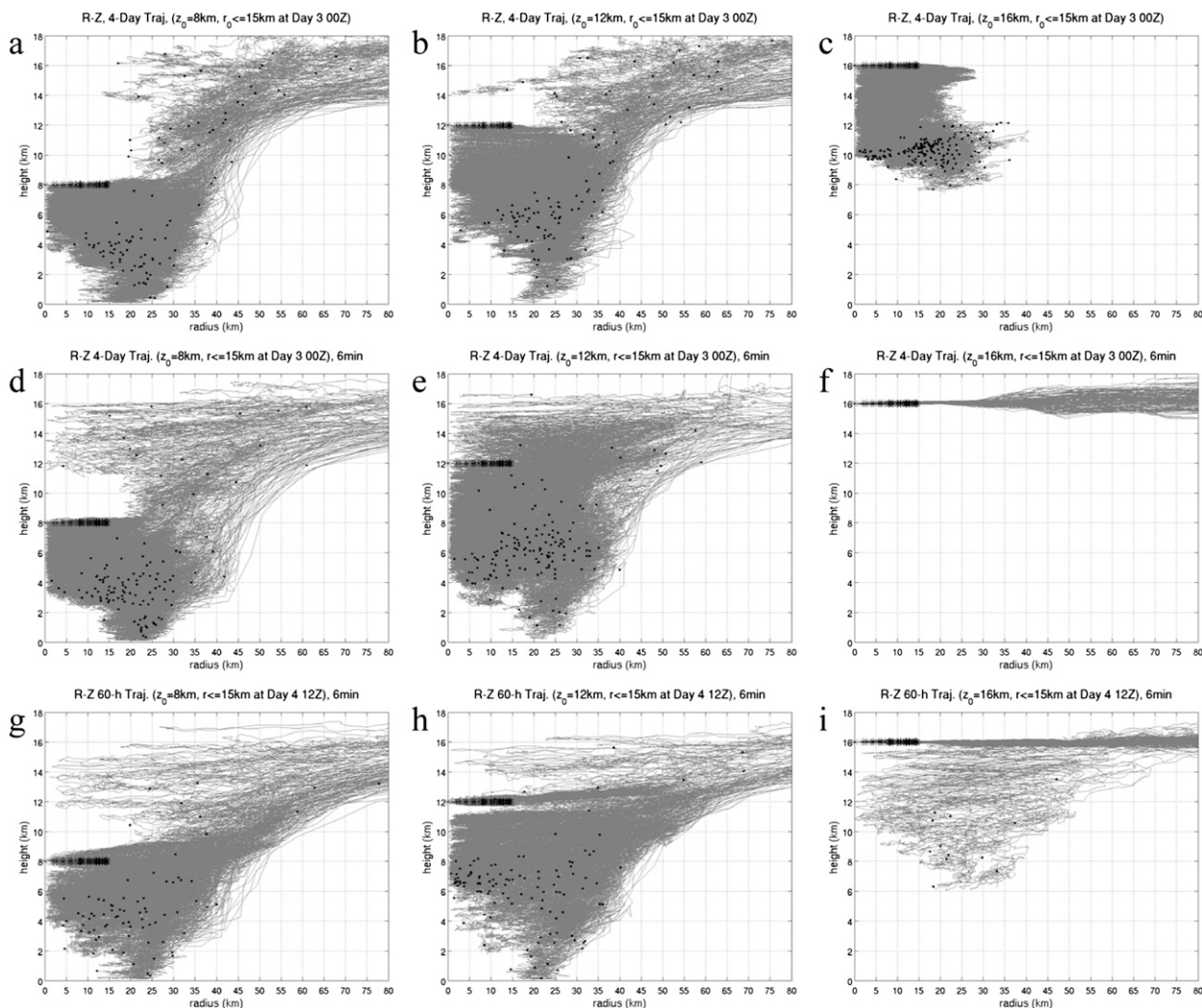


FIG. 18. Radius–height views of forward trajectories which are initiated within 15 km of the center, seeded at (a),(d),(g) 8-, (b),(e),(h) 12-, and (c),(f),(i) 16-km height. For (top) NOFLOW and (middle) SHEAR5, trajectories are 96 h and begin at 0000 UTC day 3. For (bottom) SHEAR10, trajectories are 60 h and begin at 1200 UTC day 4. The initial and final locations of each trajectory are indicated by the black asterisks and dots, respectively.

tend to be followed by a return toward the center. The large difference in behavior at 16 km is due to the fact that the circulation rapidly weakens with height at upper levels, and so at this height, azimuthal advection is so weak that most parcels are unable to reach the inflow region before exiting the eye. Excluding this region near the very top of the storm, it appears possible for parcels to descend through great depths while remaining inside the eye, even in the presence of significant vertical wind shear.

To determine the likelihood of parcels descending through a large depth while remaining inside the eye, we first examine the radius versus height of all trajectories originating within 15 km of the center, starting at 8-, 12-,

and 16-km height, for each of the simulations (Fig. 18). For 8 and 12 km in NOFLOW, many parcels at some point are entrained into the eyewall updraft, although a substantial fraction is found within the eye at all times. Some parcels are able to descend near the center to about 4 km, and some parcels descend all the way to the surface in the eye–eyewall interface region. All parcels originating at 16-km height remain within the eye throughout the 4-day period, and most descend to around 10-km height. At 8 and 12 km, the sheared simulations appear similar to NOFLOW, except that there are more parcels at 8 km that return toward the center of the upper-level (12–16 km) eye after first rising in the eyewall. At 16 km, nearly all parcels in both sheared simulations

quickly leave the eye,⁷ which is in stark contrast to NOFLOW.

To quantify the distance that a typical parcel is able to descend within the eye, it is relevant to examine the maximum negative displacement (at any time) for each trajectory, and so we made histograms of this quantity (not shown) for the trajectories shown in Fig. 18. For 8-km height in NOFLOW, the mode of the histogram is 2.25–2.50 km, although 42.6% descend by greater than 4 km. For both 12 and 16 km, the majority of trajectories experience maximum descent of greater than 6 km. Therefore, for a tropical cyclone in a quiescent environment, it is typical for parcels originating in the upper troposphere to remain in the eye for at least a few days, and to descend through a large depth of the troposphere, with some parcels descending all the way to the surface within the eye. At 8 and 12 km, the distribution of maximum displacement is similar in the sheared simulations to that in NOFLOW. Even in SHEAR10, in which the trajectories are only for 60 h, many parcels can descend by 5–10 km. Somewhat remarkably, it is also typical for parcels to descend through great depths while remaining inside the eye in a sheared environment (in a sufficiently intense storm), except for parcels originating near the very top of the storm.

4. Summary and discussion

a. Summary

In Part II of our study, we have used idealized simulations to investigate the influence of vertical wind shear on the structure of warming and descent in the eye of tropical cyclones. In Part I, we showed that the maximum perturbation temperature of a TC in a quiescent environment (NOFLOW) was found at midlevels (4–8 km), and that this was due to the fact that the rate of warming tends to be greatest in this region during the period of rapid intensification. This preferred midlevel maximum was consistent with the results of SN12, who examined 15 different simulations, all with 5 m s^{-1} environmental flow, but without shear. In SN12, we also explained that for a number of reasons (primarily the insufficient resolution of the satellite-derived temperature estimates), the conclusion of Knaff et al. (2004) that the height of the warm-core maximum decreases systematically with increasing wind shear may be incorrect. Here, we have shown that the presence of weak to

moderate shear does not systematically alter the height of the warm-core maximum in simulations; it remains at midlevels in both 5 and 10 m s^{-1} of westerly shear (SHEAR5 and SHEAR10, respectively). Furthermore, shear does not qualitatively change the distribution of the potential temperature tendencies from the various terms that combine to determine the structure of the warm core.

Through our trajectory analysis, we have addressed several outstanding questions regarding the character of descent in the eye of tropical cyclones. In all of our simulations, we found that the degree to which parcels initially near the center are stirred into the eyewall on short timescales (<12 h) varies greatly with time and height, and is apparently a strong function of intensity. At the beginning of RI (but when the storm is still weak), parcels in the midlevel eye are easily stirred into the eyewall. Once a sufficient intensity is reached ($\sim 35\text{--}45 \text{ m s}^{-1}$), however, most parcels originating near the center of the eye will remain inside the eye for a very long period, in some cases at least 3–4 days. Consequently, many parcels initially in the upper troposphere are able to descend by 5–10 km while remaining inside the eye. These results remain valid even in SHEAR10, as the behavior of eye trajectories is relatively insensitive to the presence of shear.

b. Discussion

Both with and without shear, the time-averaged azimuthal-mean descent in the eye tends to be strongest at 12–13-km height. As discussed in Part I, this is also the height at which static stability is minimized, and so warming from vertical advection is not generally maximized in upper levels. We note that this upper-level maximum in descent is inconsistent with several existing theoretical studies. Malkus (1958) hypothesized that eye descent is strongest at 1-km height, with the magnitude decreasing upward. Willoughby (1998) also assumed that descent is maximized at low levels (at the height of the temperature inversion), and decreases monotonically (and perhaps linearly) to zero at the tropopause. Both authors were attempting to explain the origin of observed eye soundings, based on combinations of descent, mixing with the eyewall, and evaporation of precipitation into subsaturated air. There are very few observational estimates of mean descent in the eye [Franklin et al. (1988) provide one such example], and none that can answer the question of where descent is vertically maximized. As our simulations are reasonably realistic in several other respects, we believe that the above theoretical estimates may be incorrect. This also raises questions about the overall utility of using soundings to infer the structure of unobserved dynamical processes.

⁷ Although it might appear from the density of lines in the figure that there is a substantial number of parcels remaining near the center in SHEAR10, there are actually only 15 (8.5%) parcels that remain within 100 km of the surface center after 24 h.

The question of why the mean descent in simulated TCs appears to be strongest at upper levels during RI is an interesting one, which we plan to address in a future study.

One of the more striking conclusions of this study is that stirring between the eye and eyewall strongly decreases with increasing intensity, irrespective of shear. The relationship between stirring and intensity is somewhat intuitive, although as far as we are aware, this is the first study to directly demonstrate this for tropical cyclones. One possible interpretation of this abrupt change in behavior as the TC develops is that it is a consequence of eye formation. However, the timing of eye formation is rather ambiguous and without a well-accepted dynamical definition [see Vigh et al. (2012) for an excellent discussion], so we think it is more useful to think in terms of intensity and/or inertial stability: As intensity rapidly increases, so does inertial stability, and therefore radial displacements into the eye become increasingly difficult. The presence of significant vertical wind shear only slightly increases the degree of stirring, and so the dominant effect of intensity is evident.

It is quite possible for parcels to descend within the eye from the upper troposphere by 5–10 km, even in the presence of 10 m s^{-1} of environmental vertical wind shear. This is accomplished by a mean descent of a few centimeters per second over several days. The parcels that descend the farthest tend to, at some point, enter the region of concentrated descent at the eye–eyewall interface, and those that reach the top of the boundary layer are often entrained therefrom into the eyewall updraft. In contrast to the mean structure, at any given moment, there are numerous updrafts and downdrafts within the eye, with magnitudes as large as 1 or 2 m s^{-1} . These are presumably the signature of transient inertia–gravity waves (e.g., Liu et al. 1999), whose amplitude is an order of magnitude larger than the mean vertical velocity. There is essentially no relationship between the strength or even the sign of the vertical velocity of a parcel and the degree to which it experiences net descent over a longer period.

At first glance, there seems to be a discrepancy between our results and those of Cram et al. (2007), who found a residence time of just a few hours for parcels in a hurricane within strong shear. However, the simulated storm in their study had an intensity of about $45\text{--}50 \text{ m s}^{-1}$, and in our simulations, this intensity corresponds to the end of the period where there is a rapid change in trajectory behavior. Furthermore, the shear in their simulation was about 12 m s^{-1} , somewhat stronger than in our SHEAR10, and so the influence of shear on eye residence time is expected to be greater in their case. Perhaps most importantly, the seed locations of eye

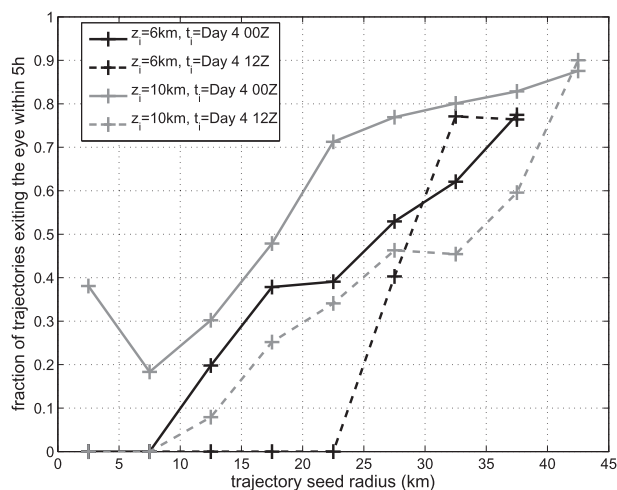


FIG. 19. Fraction of forward trajectories that exit the eye within 5 h, as a function of initial radius. Trajectories are seeded uniformly within the eye. For initial heights of 6 and 10 km, trajectories are considered to have exited the eye when their radius exceeds 40 and 47 km, respectively.

trajectories in Cram et al. (2007) extended to the outer edge of the eye (40-km radius at 6-km height), whereas we seeded only inside 15 km. Because of the increasing area with radius, their statistics are dominated by parcels seeded at the outer edge of the eye. They found that the stirring decreased with decreasing initial radius, and it can be seen (their Fig. 15) that inside 15-km radius at 5.6-km height, fewer than 20% of parcels were stirred into the eyewall within 5 h.

To further assess the above hypothesis regarding differences between our study and that of Cram et al. (2007), we extended the seeding region to the entire eye and examined the dependence of stirring on seed radius in SHEAR10, for 5-h trajectories initiated at two different times and heights (Fig. 19).⁸ Over the entire eye, the percentage of parcels seeded at 6-km height at 0000 and 1200 UTC day 4 that enter the eyewall within 5 h is 50.8% and 40.5%, respectively. For trajectories seeded at 10-km height, the percentage of such parcels entering the eyewall within 5 h is 72.1% and 50.1%, respectively. These statistics are quite similar to those found by Cram et al. (2007). Further, the percentage of eye parcels stirred into the eyewall decreases rapidly with decreasing seed radius, and nearly all trajectories

⁸ The $V_{\max 10}$ in SHEAR10 at 0000 and 1200 UTC day 4 is 42.1 and 53.0 m s^{-1} , and P_{\min} is 974.6 and 961.3 mb , respectively. For comparison, during the period examined by Cram et al. (2007), P_{\min} in the simulated Bonnie varied from 952 to 959 mb , and the maximum wind speed at the lowest model level ($z = 40 \text{ m}$) varied from about 48 to 55 m s^{-1} .

initiated near the storm center remain within the eye during this period. Therefore, our results are not necessarily inconsistent with those of Cram et al. (2007). Nevertheless, our emphasis and interpretation remain somewhat different. Evaluating Willoughby's (1998) "containment vessel" hypothesis, they concluded that in their simulation most of the air originating in the mid- and upper-level eye was not being "contained." While this is technically true, it is quite possible that a large number of the trajectories seeded near the center of the eye would remain there for many hours (if not days), were their calculations extended. We believe that for a sufficient intensity, the containment vessel hypothesis is generally correct, even in significant vertical wind shear. We note that these results apply for weak- to moderately sheared storms, and it remains possible that in shear stronger than that examined (10 m s^{-1}), the sensitivity of eye-eyewall stirring to shear becomes qualitatively different.

Our results are useful for understanding the degree to which the eye can remain isolated from the eyewall, and they indicate something fundamental about the manner in which the development and maintenance of the eye of tropical cyclones occurs. In particular, it appears that the hypothesis (Willoughby 1998) that parcels cannot be displaced vertically by more than a few kilometers within the eye need not be true, as large displacements occur quite commonly in our simulations. Part of Willoughby's (1998) objection to this possibility is that were this to occur, the air within the eye would be much drier and warmer than is ever observed. In our simulation, such unrealistic properties do not occur because θ is not conserved. Instead, θ decreases because of horizontal diffusion in the interior of the eye, and this is enhanced by sublimative and evaporative cooling at the eye-eyewall interface. One need not invoke an "unrealistic" magnitude of eye-eyewall stirring for this to occur. If a parcel descends within the eye while conserving its θ , it will on average find itself surrounded by cooler parcels, and the greater the temperature difference, the more diffusion will act to remove this perturbation. Therefore, it is clear from both our budget and trajectory analyses that diffusion is a key process in allowing for large net descent within the eye.

As mentioned in Part I, the realism of parameterized diffusion in simulations remains uncertain. The purpose of horizontal diffusion in numerical models is to attempt to represent the effects of unresolved turbulence, and "to prevent the formation of frontal discontinuities" (Rotunno and Bryan 2012). In WRF, the horizontal eddy diffusivity is proportional to a squared mixing length l_h , and l_h is proportional to the horizontal grid spacing. For $dx = 2 \text{ km}$, $l_h = 500 \text{ m}$. The most appropriate value

for this parameter is highly uncertain. For axisymmetric simulations, Bryan (2012) found that $l_h = 1000 \text{ m}$ yielded the most realistic storms, although he stated that l_h should be smaller for three-dimensional simulations. Zhang and Montgomery (2012) used flight-level observations in four intense hurricanes to calculate l_h , and found an average eyewall value of approximately 750 m , with an estimated uncertainty of 50%. Based on these studies, it is possible that our simulations are underdiffusive, although given the large uncertainty, it seems that l_h (and the diffusion) falls within the current plausible range.

While differences in trajectory behavior between quiescent and sheared environments are relatively small for the region near the storm center, they become more significant in the eye-eyewall interface region. In NOFLOW, when the storm is very intense, many parcels descending along the eye-eyewall interface at upper levels can descend 2–3 km over 12 h. While substantial, this displacement is reduced by the fact that the parcels tend to be advected radially inwards away from the zone of strong descent. There is apparently little stirring between the eye and eyewall at upper levels in NOFLOW, as virtually all parcels originating at upper levels in the annulus of strongest descent along the eye-eyewall interface remain inside the eye after 12 h. In contrast, in moderate (5 m s^{-1}) shear, most such parcels enter the eyewall within 12 h, and this is consistent with Cram et al. (2007). Not surprisingly, in shear, there are large azimuthal asymmetries in time-averaged descent in this interface region, with the descent strongest to the west (upshear) of the center. The parcels that are initially located in the left-of-shear semicircle are far more likely to remain within the eye, however. This is because of the asymmetry in storm-relative radial flow, with inflow in the western (upshear) semicircle, and outflow in the eastern (downshear) semicircle.

We have shown that in idealized simulations, trajectories initiated near the center of the eye are relatively insensitive to the presence of vertical wind shear, those near the edge of the eye have a large sensitivity to shear, and the most important influence on trajectory behavior is storm intensity. Each of these findings can be qualitatively understood by considering the same three factors: the asymmetric storm-relative radial wind, the azimuthal-mean angular velocity, and the distance from the parcel to the eyewall. It is obvious that simply because of the closer proximity, there will be enhanced stirring of the interface region with the eyewall, as compared to the stirring between the interior of the eye and the eyewall. This is not the only reason for this behavior, however. The asymmetric storm-relative radial wind represents the flow across the storm, and all else being equal, should increase with increasing vertical wind shear. To

first order, it is given by the difference between the storm motion and the large-scale environmental flow at a given height. However, the storm itself substantially modifies the relative flow, and it does so in ways that are neither trivial to understand nor spatially uniform, as can be seen in Fig. 15d. It is clear that the upper-level relative flow is enhanced within and just inwards of the eyewall, relative to the interior of the eye. When combined with the strong azimuthal-mean radial outflow of the upper-level eyewall, this leads to an increase in stirring with increasing radius.

Observational analyses of the storm-relative flow (especially at mid- and upper levels) in the eye are rare because of the typical lack of radar scatterers near the storm center. Nevertheless, there have been a few such studies that have commented on the radial variation of storm-relative flow. From flight-level data at 850 mb, Willoughby et al. (1984) found that storm-relative environmental flow may deflect around the core of the cyclone, protecting the core from the environment. Using Doppler radar analysis, Marks et al. (1992) found that in Hurricane Norbert (1984), the storm-relative winds within the eye above 3-km height were of opposite direction to the flow outside the core, and that the "... flow pattern was reminiscent of flow around an obstacle." In contrast, Franklin et al. (1993) stated that in Hurricane Gloria (1985), the midlevel flow "... is relatively unimpeded and flows through the eyewall." However, they also found that the environmental flow was "distorted" inside the core, which they presumed to be due to convection. Finally, Black et al. (2002) suggested that convective bands beyond the eyewall can protect the core from storm-relative flow associated with shear. Based on the above studies, it seems that there is some observational support for the storm-relative flow being substantially modified within the eye.

Even the presence of significant asymmetric storm-relative flow does not ensure that trajectories actually flow through the storm, as discussed recently by Riemer and Montgomery (2011). Those authors pointed out that this "... distinction does not always seem to be clear in a number of previous studies," and that for a strong vortex, the tangential flow acts "... to significantly deflect the storm-relative asymmetric flow." For a parcel initially within the eye, the asymmetric storm-relative flow will stir the parcel into the eyewall only if the time scale associated with this radial advection is less than that associated with the orbiting of the parcel about the storm center. When the angular velocity is great enough, such parcels are unable to reach the eyewall (and hence the region of large azimuthal-mean outflow) prior to being azimuthally advected into a region of asymmetric inflow. This is largely why eye-eyewall stirring decreases

so strongly with increasing intensity. For example, in SHEAR5, the angular velocity at 6-km height and 20-km radius more than doubles between 1100 and 2300 UTC on day 2 (not shown). It is probably not a coincidence that the percentage of parcels remaining inside the eye dramatically increases during this same period.

Acknowledgments. The authors would like to thank Mark Stoelinga for help with RIP4 and David Nolan for helpful discussions. The authors also are grateful for the helpful reviews of Hugh Willoughby, Jonathan Vigh, Jason Sippel, and three anonymous reviewers. This research was partially supported by ONR (Grant N000140910526), NOAA (HFIP), and the NSF (Grants 063064 and 0840651).

REFERENCES

- Black, M. L., J. F. Gamache, F. D. Marks Jr., C. F. Samsury, and H. E. Willoughby, 2002: Eastern Pacific Hurricanes Jimena of 1991 and Olivia of 1994: The effect of vertical shear on structure and intensity. *Mon. Wea. Rev.*, **130**, 2291–2312.
- Braun, S. A., M. T. Montgomery, and Z. Pu, 2006: High-resolution simulation of Hurricane Bonnie (1998). Part I: The organization of eyewall vertical motion. *J. Atmos. Sci.*, **63**, 19–42.
- Bryan, G. H., 2012: Effects of surface exchange coefficients and turbulence length scales on the intensity and structure of numerically simulated hurricanes. *Mon. Wea. Rev.*, **140**, 1125–1143.
- Cram, T. A., J. Persing, M. T. Montgomery, and S. A. Braun, 2007: A Lagrangian trajectory view on transport and mixing processes between the eye, eyewall, and environment, using a high-resolution simulation of Hurricane Bonnie (1998). *J. Atmos. Sci.*, **64**, 1835–1856.
- Dunion, J. P., 2011: Rewriting the climatology of the tropical North Atlantic and Caribbean Sea atmosphere. *J. Climate*, **24**, 893–908.
- Frank, W. M., and E. A. Ritchie, 2001: Effects of vertical wind shear on the intensity and structure of numerically simulated hurricanes. *Mon. Wea. Rev.*, **129**, 2249–2269.
- Franklin, J. L., S. J. Lord, and F. D. Marks Jr., 1988: Dropwindsonde and radar observations of the eye of Hurricane Gloria (1985). *Mon. Wea. Rev.*, **116**, 1237–1244.
- , —, S. E. Feuer, and F. D. Marks Jr., 1993: The kinematic structure of Hurricane Gloria (1985) determined from nested analyses of dropwindsonde and Doppler radar data. *Mon. Wea. Rev.*, **121**, 2433–2451.
- Halverson, J. B., J. Simpson, G. Heymsfield, H. Pierce, T. Hock, and L. Ritchie, 2006: Warm core structure of Hurricane Erin diagnosed from high altitude dropsondes during CAMEX-4. *J. Atmos. Sci.*, **63**, 309–324.
- Holland, G. J., 1997: The maximum potential intensity of tropical cyclones. *J. Atmos. Sci.*, **54**, 2519–2541.
- Kaplan, J., and M. DeMaria, 2003: Large-scale characteristics of rapidly intensifying tropical cyclones in the North Atlantic basin. *Weather Forecasting*, **18**, 1093–1108.
- , —, and J. A. Knaff, 2010: A revised tropical cyclone rapid intensification index for the Atlantic and eastern North Pacific basins. *Weather Forecasting*, **25**, 220–241.

- Kimball, S. K., and J. L. Evans, 2002: Idealized numerical simulation of hurricane–trough interaction. *Mon. Wea. Rev.*, **130**, 2210–2227.
- Knaff, J. A., S. A. Seseske, M. DeMaria, and J. L. Demuth, 2004: On the influences of vertical wind shear on symmetric tropical cyclone structure derived from AMSU. *Mon. Wea. Rev.*, **132**, 2503–2510.
- Liu, Y., D.-L. Zhang, and M. K. Yau, 1999: A multiscale numerical study of Hurricane Andrew (1992). Part II: Kinematics and inner-core structures. *Mon. Wea. Rev.*, **127**, 2597–2616.
- Malkus, J. S., 1958: On the structure and maintenance of the mature hurricane eye. *J. Meteor.*, **15**, 337–349.
- Marks, F. D., Jr, R. A. Houze, and J. F. Gamache, 1992: Dual-aircraft investigation of the inner core of Hurricane Norbert. Part I: Kinematic structure. *J. Atmos. Sci.*, **49**, 919–942.
- Nolan, D. S., 2011: Evaluating environmental favorableness for tropical cyclogenesis by statistical analysis of threshold parameters. *J. Adv. Model. Earth Syst.*, **3**, M08001, doi:10.1029/2011MS000063.
- , and E. D. Rappin, 2008: Increased sensitivity of tropical cyclogenesis to wind shear in higher SST environments. *Geophys. Res. Lett.*, **35**, L14805, doi:10.1029/2008GL034147.
- , M. T. Montgomery, and L. D. Grasso, 2001: The wavenumber-one instability and trochoidal motion of hurricane-like vortices. *J. Atmos. Sci.*, **58**, 3243–3270.
- Rappin, E. D., and D. S. Nolan, 2012: The effect of vertical shear orientation on tropical cyclogenesis. *Quart. J. Roy. Meteor. Soc.*, **138**, 1035–1054.
- , —, and K. A. Emanuel, 2010: Thermodynamic control of tropical cyclogenesis in environments of radiative-convective equilibrium with shear. *Quart. J. Roy. Meteor. Soc.*, **136**, 1954–1971.
- Reasor, P. D., M. T. Montgomery, and L. D. Grasso, 2004: A new look at the problem of tropical cyclones in vertical shear flow: Vortex resiliency. *J. Atmos. Sci.*, **61**, 3–22.
- Riemer, M., and M. T. Montgomery, 2011: Simple kinematic models for the environmental interaction of tropical cyclones in vertical wind shear. *Atmos. Chem. Phys.*, **11**, 9395–9414.
- , —, and M. E. Nicholls, 2010: A new paradigm for intensity modification of tropical cyclones: Thermodynamic impact of vertical wind shear on the inflow layer. *Atmos. Chem. Phys.*, **10**, 3163–3188.
- Rotunno, R., and G. H. Bryan, 2012: Effects of parameterized diffusion on simulated hurricanes. *J. Atmos. Sci.*, **69**, 2284–2299.
- Schubert, W. H., C. M. Rozoff, J. L. Vigh, B. D. McNoldy, and J. P. Kossin, 2007: On the distribution of subsidence in the hurricane eye. *Quart. J. Roy. Meteor. Soc.*, **133**, 595–605.
- Stern, D. P., and D. S. Nolan, 2012: On the height of the warm core in tropical cyclones. *J. Atmos. Sci.*, **69**, 1657–1680.
- , and F. Zhang, 2013: How does the eye warm? Part I: A potential temperature budget analysis of an idealized tropical cyclone. *J. Atmos. Sci.*, **70**, 73–90.
- Stoelinga, M. T., cited 2009: A users' guide to RIP version 4.5: A program for visualizing mesoscale model output. [Available online at <http://www.mmm.ucar.edu/wrf/users/docs/ripug.htm>.]
- Tang, B., and K. Emanuel, 2012: A ventilation index for tropical cyclones. *Bull. Amer. Meteor. Soc.*, **93**, 1901–1912.
- Vigh, J. L., J. A. Knaff, and W. H. Schubert, 2012: A climatology of hurricane eye formation. *Mon. Wea. Rev.*, **140**, 1405–1426.
- Willoughby, H. E., 1998: Tropical cyclone eye thermodynamics. *Mon. Wea. Rev.*, **126**, 3053–3067.
- , F. D. Marks, and R. J. Feinberg, 1984: Stationary and moving convective bands in hurricanes. *J. Atmos. Sci.*, **41**, 3189–3211.
- Wong, M. L. M., and J. C. L. Chan, 2004: Tropical cyclone intensity in vertical wind shear. *J. Atmos. Sci.*, **61**, 1859–1876.
- Zeng, Z., Y. Wang, and C.-C. Wu, 2007: Environmental dynamical control of tropical cyclone intensity—An observational study. *Mon. Wea. Rev.*, **135**, 38–59.
- Zhang, F., and D. Tao, 2013: Effects of vertical wind shear on the predictability of tropical cyclones. *J. Atmos. Sci.*, **70**, 975–983.
- Zhang, J. A., and M. T. Montgomery, 2012: Observational estimates of the horizontal eddy diffusivity and mixing length in the low-level region of intense hurricanes. *J. Atmos. Sci.*, **69**, 1306–1316.